박 사 학 위 논 문

Glycine Decarboxylase Regulates Renal Carcinoma Progression via Interferon-Stimulated Gene Factor 3-Mediated Pathway

계 명 대 학 교 대 학 원

의 학 과

PHAM THI TUYET MAI

PHAM
THI
TUYET
MAI

지도교수 하 은 영

2025년 2월

2025년 2월

Glycine Decarboxylase Regulates Renal Carcinoma Progression via Interferon-Stimulated Gene Factor 3–Mediated Pathway

지도교수 하 은 영

이 논문을 박사학위 논문으로 제출함

2025년 2월

계 명 대 학 교 대 학 원

의학과 생화학 전공

PHAM THI TUYET MAI

PHAM THI TUYET MAI의 박사학위 논문을 인준함

주 심 서 지 혜

부 심 하 은 영

부 심 김 진 영

부 심 신 소 진

부 심 하 태 경

계 명 대 학 교 대 학 원

2 0 2 5 년 2 월

Acknowledgement

I would like to begin by expressing my gratitude to my supervisor, Professor Eunyoung Ha, for her exceptional dedication and support in guiding this thesis. Without her thoughtful advice and guidance, this work would not have been possible.

I am also grateful to Professor Ji Hae Seo and Professor Jin Young Kim for granting my work and providing me the opportunity to work in one of the most supportive and well-equipped laboratories within School of Medicine.

Lastly, my thanks also go to my laboratory members, my friends, and my family for meaningful time spending together and unwavering encouragement throughout my academic journey.

2025년 2월

PHAM THI TUYET MAI

Table of Contents

List of Table

List of Figures

1. Introduction

Renal cell carcinoma (RCC) is a commonly diagnosed cancer with steadily increasing incidence and remarkedly mobility rates (1). The survival outcomes of RCC are mostly related to cancer stages with early-stage RCC showing higher survival rates compared to advanced or metastasis RCC. Despite developments in both prognosis and treatment, the overall prognosis of RCC remains challenging (1,2). Therefore, exploring new therapeutic targets for RCC treatment is essential.

Multiple cellular processes, including cell proliferation, require nucleotides as substrates for their development. In proliferating cells, nucleotide levels are higher 5-10 times than those in resting cells (3). Moreover, previous study has suggested that the levels of nucleotides significantly elevate in human cancer cells compared to non-malignant cells (4). This elevation emphasizes the key difference in nucleotide metabolism between cancerous and normal cells. Specifically, key oncogenes such as MYC proto-oncogene, bHLH transcription factor (MYC) have been shown to enhance nucleotide synthesis by activating genes that contribute to nucleotide metabolism (5). Therefore, modulating enzymes involved in nucleotide metabolism could influence deoxynucleotide triphosphate (dNTP) pools, potentially either inhibiting or promoting cell proliferation. Besides, depleting dNTPs synthesis not only disrupts cell proliferation but also affects cellular homeostasis and chemotherapy-induced responses (6-9). Thus, finding target genes that play a crucial role in nucleotide synthesis could serve as a potential strategy for cancer treatment.

Glycine decarboxylase (GLDC) is one of the enzymes of glycine cleavage system (GCS), primarily located in mitochondria. The cleavage of glycine to serin, induced by GCS, produces one-carbon units, which can be used to generate 5,10-methylene tetrahydrofolate (5,10-meTHF). This intermediate has played a significant role in *de novo* pyrimidine biosynthesis (10). Recently, the function of GLDC in human cancer has been widely examined and its role seems to be controversial. Particularly, in hepatocellular carcinoma (HCC), GLDC acts as a tumor suppressor (11), while in prostate cancer and non-small cell lung cancer (NSCLC), it promotes tumor progression (12,13). Therefore, the function of GLDC in cancer development and progression appears to differ across cancer types.

Interferon-stimulated gene factor 3 (ISGF3) is a transcription factor composed of three components: interferon regulatory factor 9 (IRF9), signal transducer and activator of transcription 1 and 2 (STAT1 and STAT2) (14). Multiple stimuli, including interferon signaling and DNA damage (14), induce the activation of ISGF3, which is indicated by increased expression of its subunits or phosphorylation of STAT1 and STAT2. ISGF3 regulates the transcription of its target genes, known as IFN-stimulated genes (ISGs), which contribute to the regulation of various cellular processes such as apoptosis, antiviral response, senescence, and cell proliferation (14,15). A previous study reveals that some key tumor suppressor genes, including lysine demethylase 5C (KDM5C), BRCA1 associated protein 1 (BAP1), polybromo 1 (PBRM1), and SET domain containing 2 (SETD2), regulate ISGF3 complex and ultimately affect tumor growth in RCC cells (16). Another study suggests that mitochondrial stress, particularly involving mitochondrial DNA

(mtDNA), promotes ISGF3 activation (17). However, the function of ISGF3 in RCC progression has not been fully elucidated. Notably, a previous study demonstrates that GLDC is a key gene associated with susceptibility to influenza (18) and further establishes a link between GLDC and innate immune response in lung cancer cells infected with influenza. Thus, additional studies are required to investigate the possible association between GLDC and immune pathway.

In this study, I hypothesized that GLDC is involved in nucleotide synthesis, which may influence RCC progression by either inhibiting or promoting its development. Furthermore, I aimed to explore the mechanism by which GLDC contributes to RCC progression.

2. Materials and Methods

2.1. Cell culture:

ACHN, Caki-2, HEK293T, and A498 cells were obtained from the American Type Culture Collection (ATCC) (Manassas, VA, US) and cultured in DMEM high glucose medium (Welgene, Gyeongsangbuk-do, Korea) supplemented with 1% penicillin-streptomycin (Gibco, Grand Island, NY, USA) and 10% fetal bovine serum (FBS) (Welgene, Gyeongsangbuk-do, Korea). All the cells were maintained in a incubator at 37 ℃ and 5% CO_2.

2.2. Cell proliferation and viability assay:

Cells were plated into 96-well plates. For cell proliferation assay, proliferation rate was assessed using Cell Counting Kit-8 (CCK8) (Dojindo, Kumamoto, Japan) from 0 to 5 days after seeding. For cell viability assay, cells were treated with cisplatin (CP) (Sigma-Aldrich, St.Louis, MO, USA) for 24 or 48 h, or with doxorubicin (Dox) (Sigma-Aldrich, St.Louis, MO, USA) for 12 or 24 h. Cell viability was then measured using CCK8 (Dojindo, Kumamoto, Japan) at the indicated time points.

2.3. Colony formation:

Cells were plated into 12-well or 6-well plates and grown for 1-2 weeks. Cells were then fixed with 4% paraformaldehyde (PFA)

(Thermo-Scientific, Boston, MA, USA). After that, 0.05% crystal violet (Sigma-Aldrich, St.Louis, MO, USA) was used to stain cells for 15 min. The staining intensity was assessed by adding methanol for 5 min and measured at the wavelength of 570 nm.

2.4. Cell transfection and stable cell generation:

Cells were transfected with siRNA of negative control (siNC) (Bioneer, Daejeon, Korea), STAT2 or IRF9 by Oligofectamin (Invitrogen, Waltham, MO, USA) or Lipofectamin 2000 (Invitrogen, Waltham, MO, USA) following the instructions of manufacturers. Then, cells were collected 24 h or 48 h after transfection to extract protein or mRNA to evaluate transfection efficiency.

For establishment of stably transfected cells, plasmids for short hairpin RNA (shRNA) of GLDC (shGLDC) and corresponding control vector (CTL) were purchased from Sigma-Aldrich (St.Louis, MO, USA). Overexpression plasmid for GLDC (OE GLDC) and its corresponding control vector (EV) were purchased from Addgene (Watertown, MA, USA). These plasmids were transfected into HEK293T cells to produce lentivirus. After 48 h of transfection, the media containing lentivirus was harvested and transfected to target cells using polybrene (Sigma-Aldrich, St.Louis, MO, USA) overnight. Then, target cells were maintained in fresh media for the next 48 h. Puromycin (Gibco, Grand Island, NY, USA) at concentrations of 1-10 μg/mL was used to select cells expressing transfected genes until colonies of cells became visible. To further verify the transfection efficiency, protein levels and mRNA levels of target genes were evaluated.

2.5. Wound healing assay:

Cells were grown in 12-well or 6-well plates. A ten μL pipette tip was used to generate the wound. Images of cells were captured at 0 h and 24 h under the microscope (CKX53, Olympus, Tokyo, Japan). To determine wound healing rate, ImageJ software (National Institutes of Health, Bethesda, MD, USA) was used to measure wound areas.

2.6. Cell migration assay:

Transwell chambers (Corning, Tewksbury, MA, USA) were used to perform migration. Cells were seeded in the upper chamber with serum-free medium. The lower chamber was added with fresh medium containing 10% FBS (Welgene, Gyeongsangbuk-do, Korea). After 24 h of migration, cells were harvested and fixed with 4% PFA (Thermo-Scientific, Boston, MA, USA). The invaded cells were stained with crystal violet (Sigma-Aldrich, St.Louis, MO, USA) and images were captured under the microscope (CKX53, Olympus, Tokyo, Japan).

2.7. Western blot (WB):

Cells were lysed using radioimmunoprecipitation assay (RIPA) buffer (Elpis Biotech, Daejeon, Korea) containing 1% phenylmethylsulfonyl fluoride (PMSF) (Cell Signaling Technology, Danvers, MA, USA) and 1% protease inhibitor cocktail (Gendepot, Katy, TX, USA). Then, cells were centrifuged at 13,000 rpm for 20

min at 4 ℃ to remove cell pellet. Protein concentration was determined using bicinchoninic acid (BCA) Protein Assay Kit (Thermo Scientific, Boston, MA, USA). The same amounts of proteins were loaded and separated using sodium dodecyl sulfate polyacrylamide gel electrophoresis (SDS-PAGE). Then, proteins were transferred to polyvinylidene difluoride (PVDF) membrane (GE Healhcare, Little Chalfont, UK) and blocked with skim milk for 1 h. After blocking, the membrane was exposed to primary antibody overnight at 4 ℃ and subsequently to secondary antibody for 2 h at room temperature (RT). Finally, protein expression was detected with chemiluminescence. Antibodies: GAPDH (GTX627408, GeneTex, Irvine, CA, USA), β-actin (4967S, Cell Signaling, Danvers, MA, USA), GLDC (PA5-22102, Thermo Fisher, Waltham, MA, USA), STAT2 (44-362G, Thermo Fisher, Waltham, MA, USA), IRF9 (76684, Cell Signaling, Danvers, MA, USA), STAT1 (AHO0832, Thermo Fisher, Waltham, MA, USA), H3 (4620, Cell Signaling, Danvers, MA, USA), H3K36me3 (ab9050, Abcam, Cambridge, UK), SETD2 (PA5-34934, Thermo Fisher, Waltham, MA, USA), p-H2AX (9718, Cell Signaling, Danvers, MA, USA).

2.8. Quantitative polymerase chain reaction (qPCR):

TRIzol reagent (Thermo Fisher, Waltham, MA, USA) was used to extract total RNA. The concentration and the purification of extracted RNA were determined using NanoDrop 2000 spectrophotometer (NanoDrop Technologies, Wilmington, DE, USA). Then, extracted RNA was reverse-transcribed into cDNA and applied to qPCR using SYBR Green mix (TOYOBO, Novi, MI, USA).

The reaction was conducted on a LightCycler 480 II (Roche, Basel, Switzerland).

2.9. Immunofluorescence (IF) staining:

In 24-well plates, cells were plated on coverslips. For collection, cells were fixed with 4% PFA (Thermo-Scientific, Boston, MA, USA) for 20 min. Then, cells were permeabilized with 0.1% TritonX-100 (Generay Biotech, Shanghai, China) for 10 min at RT and blocked with 1% bovine serum albumin (BSA) (Sigma-Aldrich, St. Louis, MA, USA) for 30 min. Cells were then exposed with interested primary antibody overnight at 4 ℃ and subsequently to secondary antibody for 1 h at RT. 4',6-diamidino-2-phenylindole (DAPI) (Sigma-Aldrich, St. Louis, MA, USA) was used to stain nucleus. Images were obtained using Leica Stellaris 5 confocal microscope (Leica, Wetzlar, Germany). Antibodies: lamin B1 (ab16048, Abcam, Cambridge, UK), HSP60 (12165, Cell Signaling, Danvers, MA, USA), DNA (CBL186, Sigma-Aldrich, St. Louis, MA, USA), p-H2AX (9718, Cell Signaling, Danvers, MA, USA). To quantify the nucleoid areas, 5-10 random images containing approximately 50-100 nucleoids were captured. The nucleoid areas were then calculated using ImageJ software (National Institutes of Health, Bethesda, MD, USA).

2.10. *In vivo* mouse experiment:

The animal experiment was approved by the Institutional Animal Care and Use Committee (IACUC) of Keimyung University, School of Medicine, Daegu, Korea (KM-2020-16R1). Seven-week-old male

BALB/c nude mice were purchased from the JA Bio (Suwon, Korea) and acclimatized for 1-2 weeks before experiment. Mice were then injected subcutaneously in the flank with ACHN or A498 cells. Tumor volume (V) was measured twice a week and determined following formula: $V = 0.5 \times L \times W^2$ (L: tumor length and W: tumor width).

2.11. Reactive oxygen species (ROS) measurement:

MitoSOX (Thermo Fisher, Waltham, MA, USA) was used to stain mitochondrial ROS level. After staining, the level of ROS was determined using fluorescence-activated cell sorting (FACS) analysis or by measuring the fluorescence intensity of images captured with a Leica Stellaris 5 confocal microscope (Leica, Wetzlar, Germany).

2.12. Immunohistochemistry (IHC):

Tumor tissues were sectioned into four-μm-thick paraffin slides, deparaffinized, and rehydrated. Then, they were applied to heat-induced antigen retrieval and blocked with goat serum. Next, the slides were exposed to primary antibody overnight at 4 ℃ and subsequently with secondary antibody for 30 min at RT. Diaminobenzidine chromogen (DAB) (Vector Laboratories, Newark, CA, USA) was used for signal visualization, followed by hematoxylin counterstaining. The slides were analyzed under a Leica microscope (DM750, Leica, Wetzlar, Germany).

2.13. Measurement of deoxynucleotide triphosphates

(dNTPs):

Same number of cells in the log-phase growth were collected and placed in 500 μL of ice-cold 60% methanol. Cells were then lysed by sonication for 30 s, heated at 95 ℃ for 3 min, and centrifuged at 18,500 x g for 6 min at 4 ℃ to obtain supernatant, which was then subjected to Amicon Ultra-0.5-mL centrifugal filters (Merck Millipore, Burlington, MA, USA). The extract was used to measure dNTP levels following a described previously protocol (19). In brief, single-stranded dNTP detection template binds with detection primer at 3' primer-binding site, followed by a single detection site for quantified dNTP. The remaining portion of dNTP detection template does not contain any complementary base of quantified dNTP. Double-stranded DNA then binds with EvaGreeen (Biotium, Fremont, CA, USA) fluorochrome, and its fluorescence was measured. The reaction was conducted using LightCycler 480 II (Roche, Basel, Switzerland).

2.14. Statistical analyses:

All analyses were performed using GraphPad Prism 8.2.0 (GraphPad, Boston, MA, USA). All experiments were conducted independently in triplicate. Data was represented as mean ± SD. Student's *t*-test was applied to compare two groups, and one-way ANOVA was employed for comparing multiple groups. A p-value < 0.05 was considered as significant.

Table 1. Primer Sequences for Real-time PCR

Primer name	Forward (5'-3')	Reverse (5'-3')
β-actin	GGACTTCGAGCAAGAGATGG	AGCACTGTGCCCGTACAG
GLDC	GCAGTTCACCTCAAGGCCAT	CTGAGCATTCATATTTGCCC
OAS1	GTTGCCACTCTCTCTCCTGT	CACCTTGGACACACACACAG
IFIT1	GGACAGGAAGCTGAAGGAGA	GCCCTTTTGTAGCCTCCTTG
IFI44	GAGGTCTGTTTTCCAAGGGC	CGCCTTCTTTCTCACTCAGC
IFI44L	GCCAAGTAAGCCCCATATGC	ATGGGATTTGAGGGCTTCCA
CCL5	GAAAGAACCGCCAAGTGTGT	GTGGTAGAATCTGGGCCCTT
MX1	TTGACGAAGCCTGATCTGGT	CTTCTCTCTCTGCAGGGCTT
IFI27	ACCAAGTTCATCCTGGGCTC	TTGGGATAGTTGGCTCCTCG

CCL5: C-C motif chemokine ligand 5; GLDC: glycine decarboxylase; IFI27: interferon alpha-inducible protein 27; IFI44: interferon induced protein 44; IFI44L: Interferon-induced protein 44-like; IFIT1: interferon-induced protein with tetratricopeptide repeats 1; MX1: MX dynamin like GTPase 1; OAS1: 2'-5'-oligoadenylate synthetase 1.

Table 2. DNA Oligonucleotides Used in dNTPs Assay

EvaGreen based detection	Sequences in 5' to 3' direction
Detection primer	CCGCCTCCACCGCC
dTTP detection template	TCGGTCCTCGCTCGCTCTTGCCTCGGTCCTTTATTTGGCGGTGGAGGCGG
dATP detection template	ACAGACCAGAGAGACACAACAGACGGAGGAAATAAAGGCGGTGGAGGCGG
dCTP detection template	TCAATCCCCACTCACTCTTACCTCAATCCTTTGTTTGGCGGTGGAGGCGG
dGTP detection template	TGAATGATGAGTGAGTGTGAGGTGAATGGTTTCTTTGGCGGTGGAGGCGG

dATP: deoxyadenosine triphosphate; dCTP: deoxycytidine triphosphate; dGTP: deoxyguanosine triphosphate; dTTP: deoxythymidine triphosphate.

Table 3. Short Interfering RNAs (siRNA)

Gene name	Sequence
NC	ACGUGACACGUUCGGGAAUU UUCUCCGAACGUGUCACGU
STAT2	GACUCUGGACAAUCUCAC UGUGAGAUUGUCCAGAGUC
IRF9	CUCUUCAGAACCGCCUACU AGUAGGCGGUUCUGAAGAG

IRF9: interferon regulatory factor 9; NC: negative control; STAT2: signal transducer and activator of transcription 2.

3. Results

3.1. Downregulation of GLDC depletes dNTPs synthesis, leading to ROS accumulation and mitochondrial stress in RCC cells:

GLDC is one of four enzymes in GCS, which catalyzes glycine to synthesize tetrahydrofolate. This substrate has the main function in the nucleotide synthesis (20,21). Hence, this study hypothesized that downregulation of GLDC would decrease nucleotide synthesis and result in attenuation of dNTP levels. I first assessed dNTP levels in control and GLDC-depleted RCC cells and found that suppression of GLDC decreased levels of all four types of dNTP in both ACHN and Caki-2 cells (Figure 1A).

Additionally, previous studies have shown that downregulation of dihydroorotate dehydrogenase (DHODH), which inhibits intracellular nucleotide synthesis, induces ROS generation (22,23). Here, ROS level in RCC cells was evaluated following the treatment of Brequinar (Bre), a DHODH inhibitor. The result demonstrated that ROS production was significantly increased in ACHN cells treated with Bre (Figure 1B). Consistently, knockdown of GLDC augmented ROS accumulation in both ACHN and Caki-2 cells (Figure 1C). These results suggest that suppression of GLDC inhibits nucleotide synthesis, which leads to ROS accumulation in RCC cells.

The elevation of ROS level might lead to mitochondrial stress and dysfunction. Mitochondrial stress includes the enlargement of nucleoid-mtDNA-and the release of mtDNA into cytosol, resulting in

promotion of cyclic GMP-AMP synthase-stimulator of interferon genes (cGAS-STING) pathway to increase expression of ISGs (17,24). Accordingly, to determine whether knockdown of GLDC affects mtDNA, cells were stained with heat shock protein (HSP60), a mitochondrial marker, and DNA to evaluate the size of nucleoids. Interestingly, IF analysis revealed that GLDC depletion generated enlarged nucleoids in ACHN cells (Figure 2). This result suggests that elevated ROS generation following the depletion of GLDC may induce mitochondrial stress.

3.2. Knockdown of GLDC decreases RCC cell proliferation, colony formation, and sphere formation:

With GLDC knockdown inhibiting nucleotide synthesis, I hypothesized that knockdown of GLDC could impact RCC cell progression. To investigate this, I established ACHN and Caki-2 cells with stable GLDC knockdown as well as A498 cells with GLDC overexpression. I found that cell proliferation was diminished in GLDC-depleted cells compared to control cells (Figure 3A). Consistently, colony assay revealed that colony formation was significantly decreased in ACHN and Caki-2 cells with GLDC knockdown (Figure 3B).

To investigate the effect of GLDC on sphere formation, I performed sphere assay on indicated cells. Figure 4A shows that depletion of GLDC in ACHN and Caki-2 cells reduced the number of primary spheres larger than 50 μm. Conversely, the number of spheres larger than 50 μm was higher in GLDC-overexpressing A498 cells than those in control cells (Figure 4A). However, Figure

4B&C indicate that knockdown of GLDC in ACHN cells did not show any significant changes in cell migration. Overall, I could conclude that knockdown of GLDC decreases RCC cell proliferation, colony formation, and sphere formation.

3.3. Knockdown of GLDC induces ISGF3 pathway activation:

Previous studies suggest that mtDNA damage activates ISGF3 pathway and further stimulates innate immune system (14,16,17). Based on the result showing that knockdown of GLDC induces mitochondial stress and enlarged mtDNA, I hypothesize that GLDC could regulate RCC progression via activation of ISGF3. ISGF3 is a transcription factor consisting of three subunits: STAT2, STAT1 and IRF9. Activation of ISGF3 can be initiated either by phosphorylation of STAT2 and STAT1 or by increased expression of its subunits (25). Accordingly, Figure 5A illustrates the expression of ISGF3 subunits in ACHN and Caki-2 cells. I found that knockdown of GLDC augmented protein expression of STAT2 and IRF9. In contrast, overexpression of GLDC in ACHN cells decreased expression level of these proteins. Moreover, WB analysis also reveals the increased expression of SETD2 and its downstream target, histone 3 lysine 36 trimethylation (H3K36me3), which has been proven to regulate ISGF3 (16), in GLDC-depleted cells (Figure 5A). Consistently, suppression of GLDC increased mRNA expression of ISGs target genes in ACHN and Caki-2 cells (Figure 5B).

To determine whether suppression of ISGF3 could induce any effects on GLDC-depleted cells, ACHN cells were co-transfected

with siSTAT2 and/or siIRF9. Figure 6A&B suggest that co-knockdown of STAT2 and IRF9, but not silencing STAT2 or IRF9 alone, could reverse cell proliferation and colony formation, which were previously decreased by depletion of GLDC. These results suggest that GLDC regulates RCC progression possibly via activating ISGF3 pathway.

Moreover, previous studies reveal that GLDC has an important function in regulating viral infection, which has been shown to induce the stimulation of ISGF3 pathway (18). Therefore, I used polyinosinic-polycytidylic acid (poly(I:C)), a viral infection mimic, to activate the innate immune response in ACHN cells, and found that GLDC-depleted cells exhibited significantly higher expression of interferon alpha (IFNα) compared to control cells (Figure 6C).

3.4. Inhibition of dNTPs synthesis induced by GLDC knockdown suppresses cell proliferation:

To elucidate the underlying mechanism by which GLDC knockdown activates ISGF3 pathway and subsequently regulates RCC cell proliferation, ACHN cells were treated with Bre, a DHODH inhibitor, to induce intracellular inhibition of nucleotide synthesis. Figure 7A demonstrates that treatment of Bre decreased proliferation rate in ACHN cells. In addition, there was an increased protein expression of STAT2 and IRF9 and mRNA expression of ISGs target genes in Bre treated cells (Figure 7B&C). Thus, these results suggest that inhibition of nucleotide synthesis could activate ISGF3 pathway.

To perform the rescue experiments, deoxynucleosides (dNs) were added in both control and GLDC-depleted cells to determine their

effect on RCC cell progression. Figure 8A shows that dNs addition reversed GLDC knockdown-induced ROS accumulation in ACHN cells. Moreover, addition of dNs increased cell proliferation in GLDC-depleted cells to levels comparable to those of control cells (Figure 8B). Indeed, dNs addition decreased expression of STAT2 and IRF9 in GLDC-deficient cells (Figure 8C). Overall, I can conclude that knockdown of GLDC suppresses nucleotide synthesis, which later decreases cell proliferation through ISGF3 activation.

3.5. Depletion of GLDC augments cell death and DNA damage induced by Dox or CP in RCC cells:

Previous studies suggest that suppression of nucleotide synthesis increases anticancer drug-induced double strand breaks (DBSs) (9). Additionally, SETD2 has a crucial function in the regulation of the induction and repair of DBSs in RCC cells (26). Given the results that knockdown of GLDC reduced dNTP pools and increased SETD2 expression, I hypothesized that GLDC could be involved in the cellular response to chemotherapy-induced DNA damage. To test this hypothesis, I treated chemotherapy drug, Dox or CP, to induce DNA damage, and found that cells with GLDC knockdown exhibited lower viability following treatment of Dox or CP compared to control cells (Figure 9A&B).

To observe DNA damage induced by chemotherapy, cells were stained with p-H2AX, a DNA damage marker. Figure 10A shows that p-H2AX expression appeared earlier and lasted longer in GLDC-depleted cells than in control cells. Specifically, after releasing cells into fresh media for 24 h, the signals of p-H2AX in

GLDC-depleted cells were still expressed, while no significant signal was detected in control cells at the same time point. Corroborating with this result, protein expression of p-H2AX was higher in GLDC-depleted cells at all time points (Figure 10B). Thus, these results demonstrate that knockdown of GLDC aggravates Dox or CP-induced DNA damage and lengthens DNA repair process.

3.6. Knockdown of ISGF3 subunits reduces Dox or CP-induced DNA damage in GLDC-deficient cells:

To investigate whether ISGF3 activation could contribute to cellular response to DNA damage in GLDC-deficient cells. Cells were treated with Dox or CP following knockdown STAT2 and/or IRF9. Figure 11A shows that decreased expression of STAT2 and/or IRF9 diminished Dox or CP-induced cell death in GLDC-depleted cells. Furthermore, I also observed that knockdown of STAT2 and/or IRF9 dampened the long-lasting damage induced by Dox or CP in GLDC-deficient cells (Figure 11B). These results suggest that ISGF3 contributes to the augmented DNA damage and longer repair in GLDC-depleted cells.

3.7. Knockdown of GLDC alleviates p53-dependent cell cycle checkpoint in response to DNA damage and aggravates mitotic catastrophe induced by Dox in RCC cells:

Cellular response to DNA damage involves the activation of p53-dependent pathway to arrest cells and further facilitate DNA

repair (27). Figure 12A shows that treatment of Dox induced expression of p53 and its downstream p21 as well as its phosphorylation form in both control and GLDC-deficient cells. However, expression of indicated proteins were remarkably higher and lasted longer in control cells than those in GLDC-depleted cells (Figure 12A). Interestingly, cell cycle analysis suggested that control cells exhibited a higher number of cells arrested in G2/M phase than those in GLDC-deficient cells (Figure 12B). These results demonstrate that GLDC depletion alleviates the activation of p53 pathway to arrest cells for further repair.

Given that cells with DNA damage fail to arrest cell cycle for repair, they may undergo mitotic catastrophe, ultimately leading to cell death. Mitotic catastrophe cells were observed by performing lamin B1 IF staining to examine nuclear morphology. Cells with mitotic catastrophe are identified by micro-nuclei (abnormal interphase), which differentiates them from normal mono-nucleated cells (normal interphase). Figure 13 illustrates that GLDC-depleted cells displayed a higher percentage of cells undergoing mitotic catastrophe compared to control cells. This result was consistent with the finding from cell cycle analysis.

3.8. GLDC regulates RCC progression *in vivo*:

To elucidate the role of GLDC *in vivo* model, GLDC-depleted cells and GLDC-overexpressing cells were injected subcutaneously into the flanks of nude mice. Figure 14A-C suggest that GLDC-depleted ACHN cells showed a decreased tumor volume and tumor weight compared to control cells, while GLDC-overexpressing A498 cells

exhibited higher tumor volume and tumor weight compared to corresponding control cells. Expression of GLDC and ISGF3 subunits were confirmed by IHC and WB analysis (Figure 14D&E). Interestingly, Figure 14D reveals that Ki67, a proliferation marker, markedly decreased in tumors derived from GLDC-deficient cells. Overall, these findings determine that GLDC acts as an oncogene in RCC progression and it might serve as a promising target for RCC therapy.

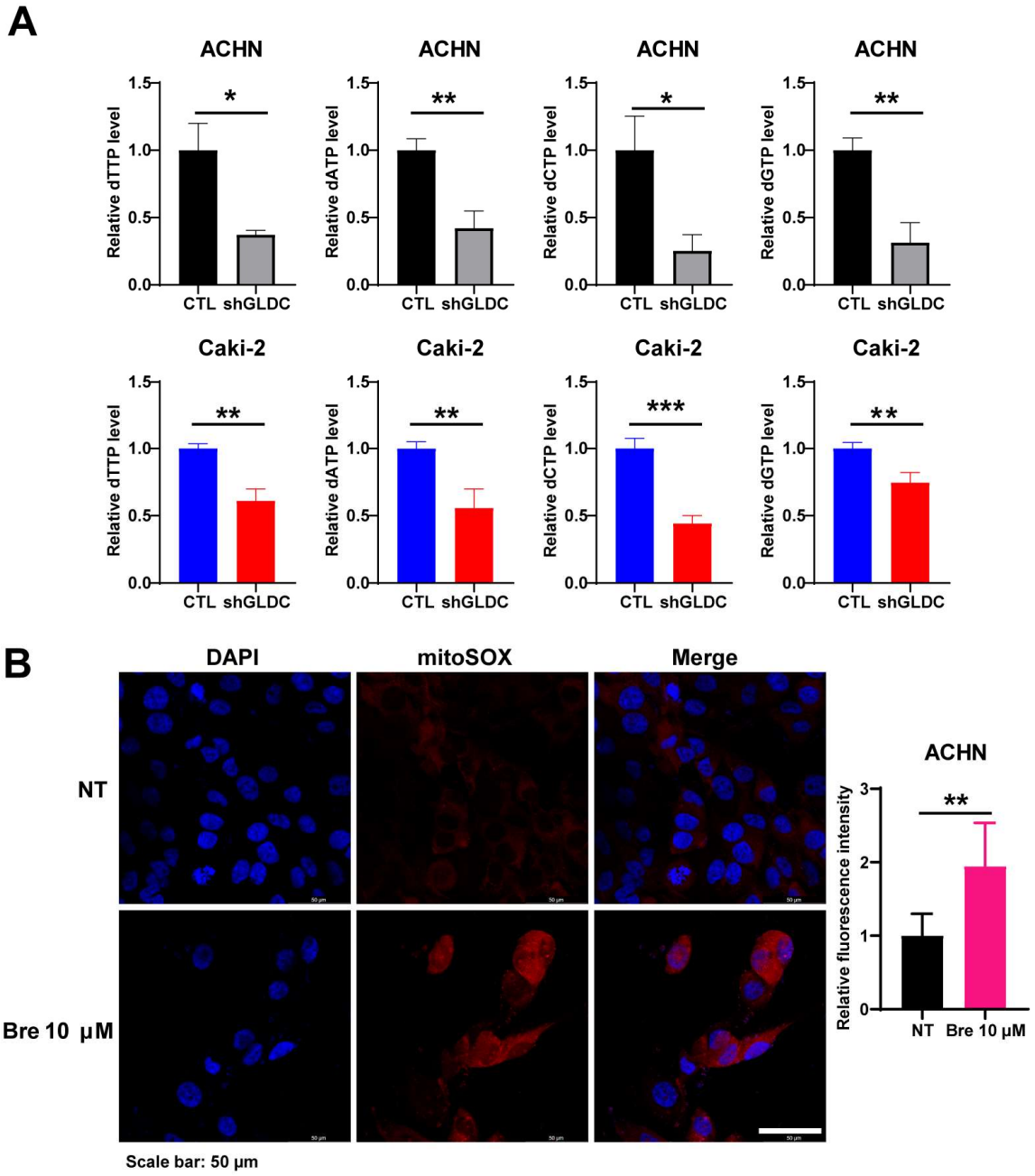

(continued)

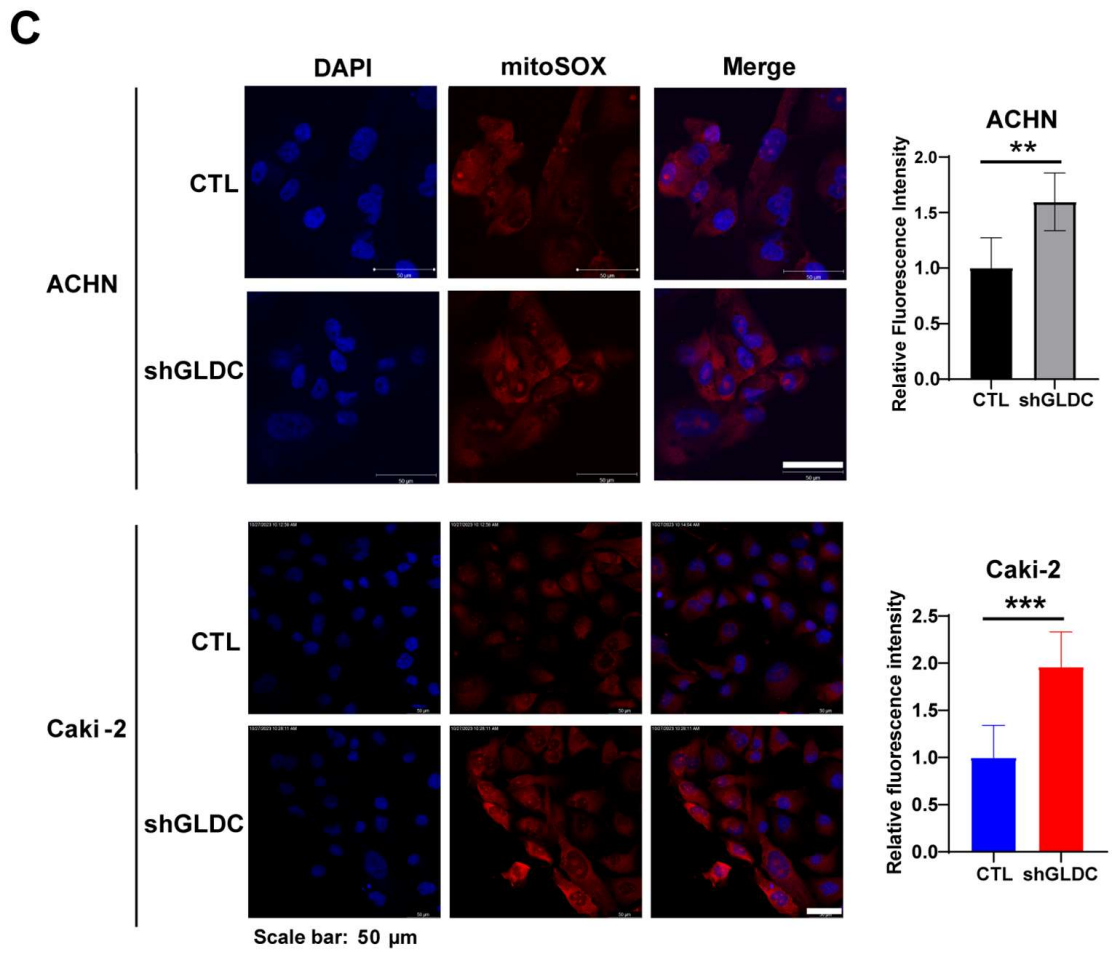

Figure 1. Downregulation of GLDC depletes dNTPs synthesis, leading to ROS accumulation. (A) Quantitative levels of dTTP, dATP, dCTP, and dGTP in ACHN and Caki-2 cells. (B) Representative images of mitoSOX staining in ACHN cell treated with Bre 10 μM for 48 h. Quantification of fluorescence intensities was performed using ImageJ. (C) Representative fluorescence images of mitoSOX staining in ACHN and Caki-2 cells. Data are represented as the mean ± SD (n = 3). Significant levels are indicated as follows: * $p < 0.05$, ** $p < 0.01$, and *** $p < 0.001$. Bre: brequinar; CTL: control; DAPI: 4',6-diamidino-2-phenylindole; NT:

non-treatment; shGLDC: knockdown of GLDC.

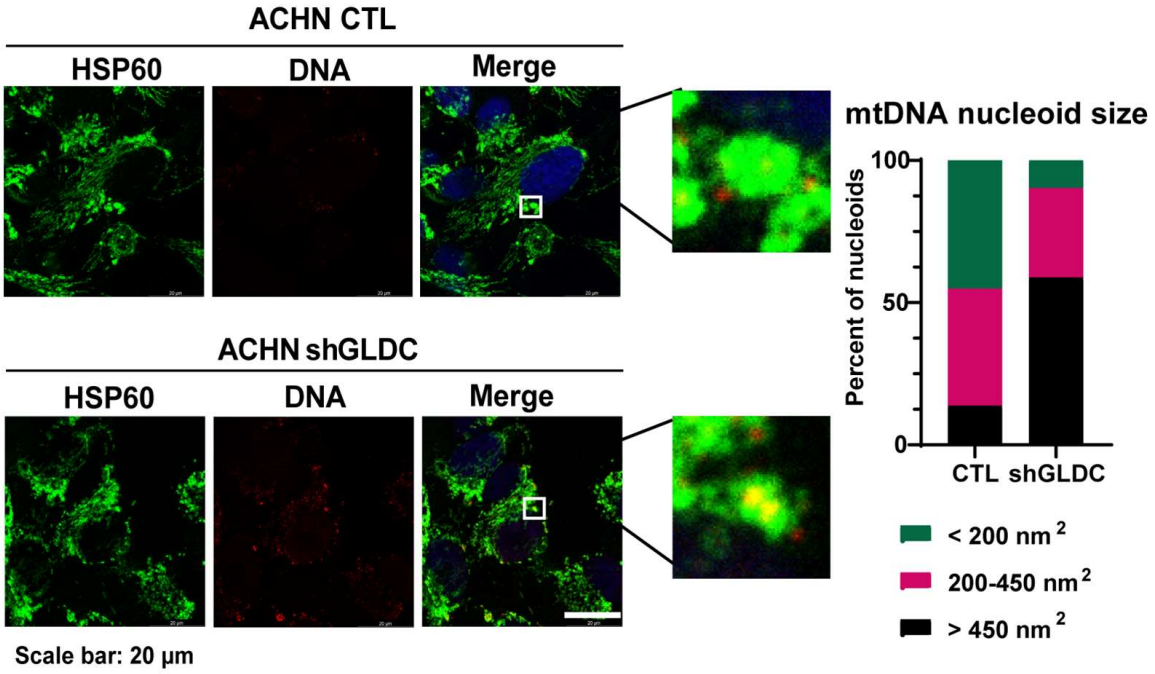

Figure 2. ROS elevation induced by GLDC depletion results in mitochondrial stress. Representative fluorescence images of cells staining with HSP60 and DNA to observe nucleoids of mitochondria. Quantification of nucleoid sizes was performed using ImageJ. CTL: control; HSP60: heat shock protein 60; mtDNA: mitochondrial DNA; shGLDC: knockdown of GLDC.

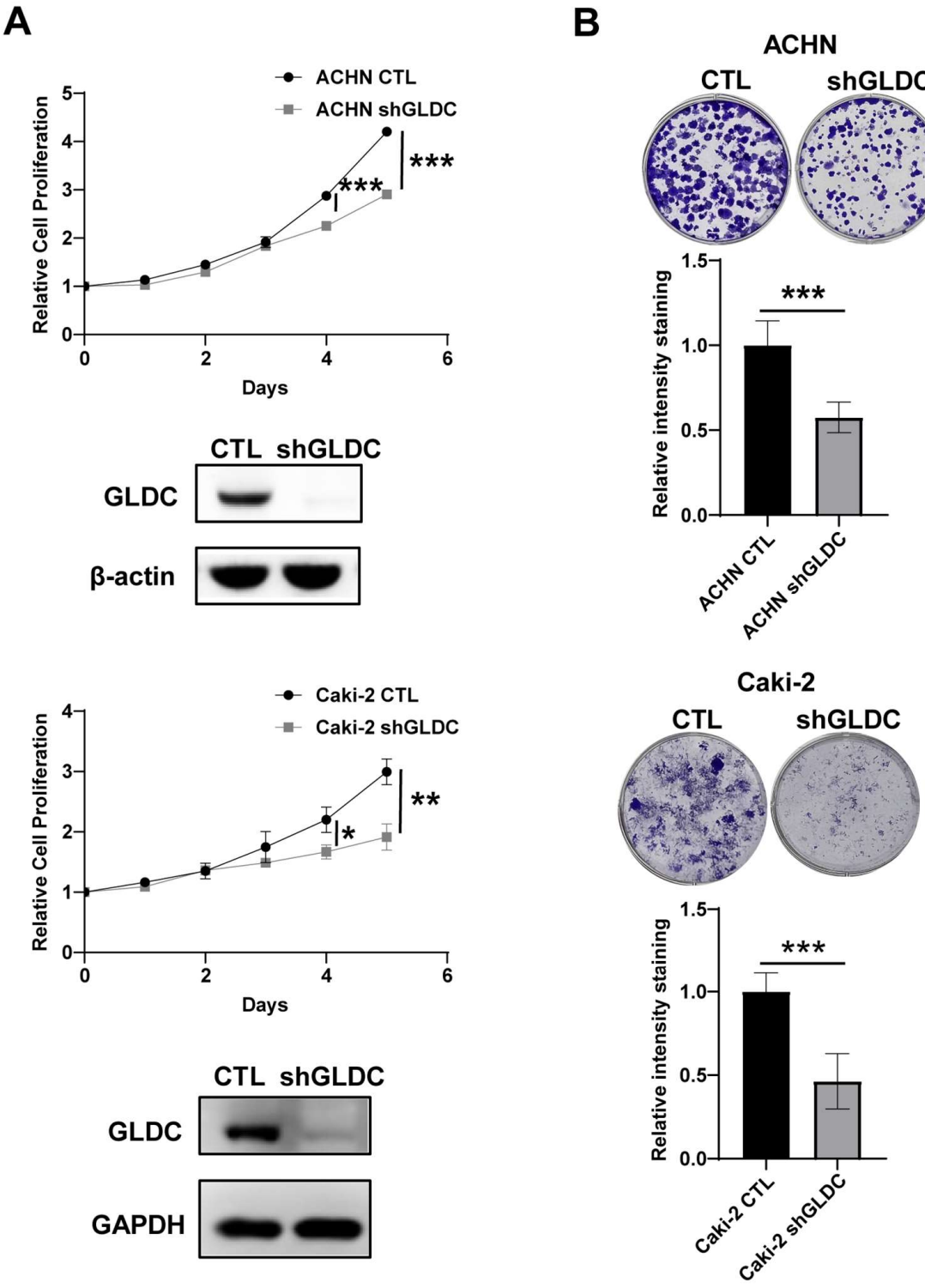

Figure 3. Knockdown of GLDC decreases RCC cell proliferation and colony formation. (A) Cell proliferation of ACHN and

Caki-2 cells. (B) Colony formation of indicated cells. Data are represented as the mean ± SD (n = 3). Significant levels are indicated as follows: * $p < 0.05$, ** $p < 0.01$, and *** $p < 0.001$. CTL: control; shGLDC: knockdown of GLDC.

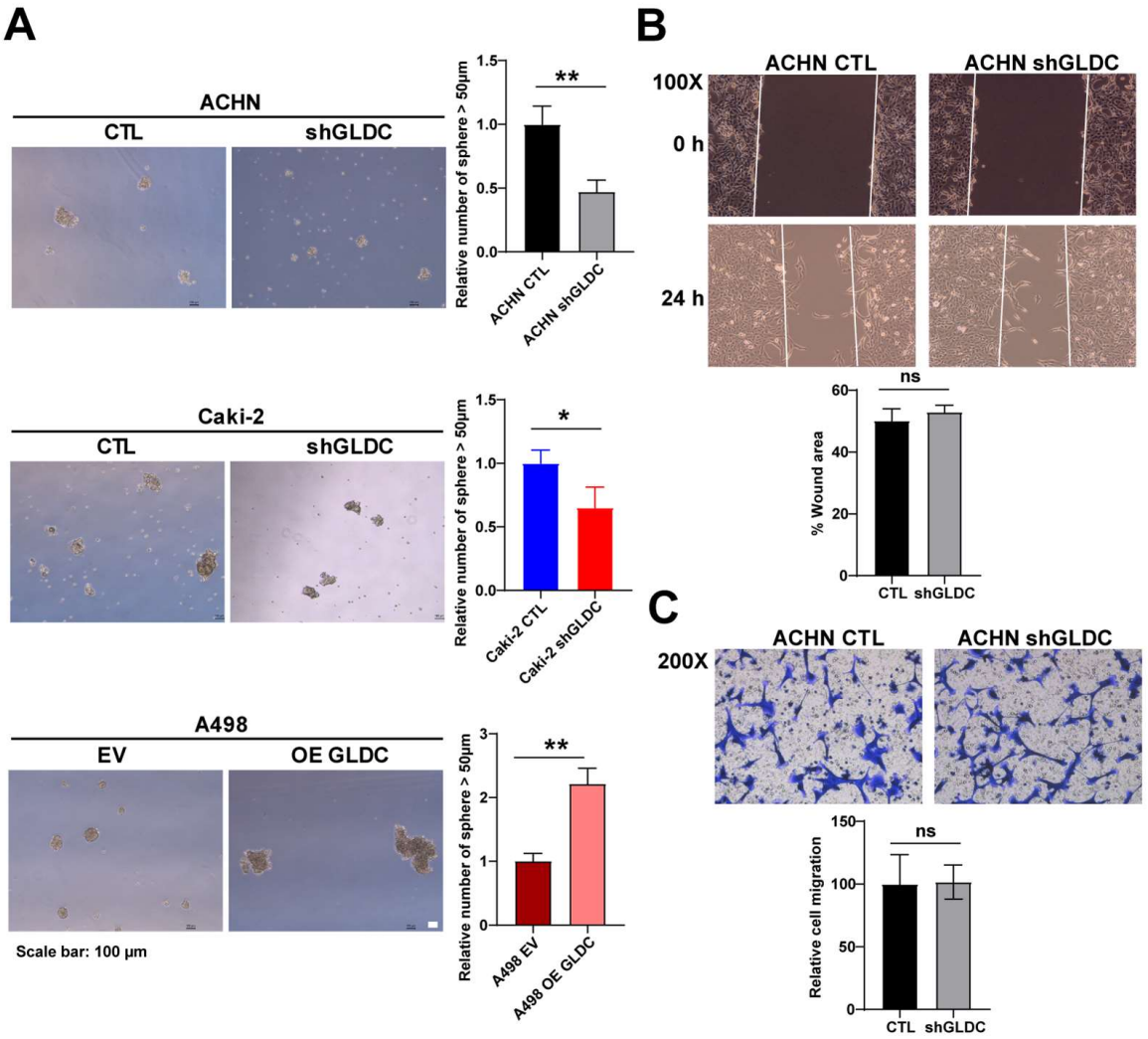

Figure 4. Knockdown of GLDC decreases RCC sphere formation but not cell migration. (A) Primary sphere formation of RCC cells. ImageJ was used to determine the size of spheres. (B) Wound healing assay of ACHN CTL and shGLDC cells. Wound areas were captured at 0 and 24 h after scratching and measured using ImageJ. (C) Cell migration assay of ACHN CTL and shGLDC cells. Data are represented as the mean ± SD (n = 3). Significant levels are indicated as follows: * $p < 0.05$, ** $p < 0.01$, and ns: not significant.

CTL: control; EV: corresponding control of OE GLDC; OE: overexpression of GLDC; shGLDC: knockdown of GLDC.

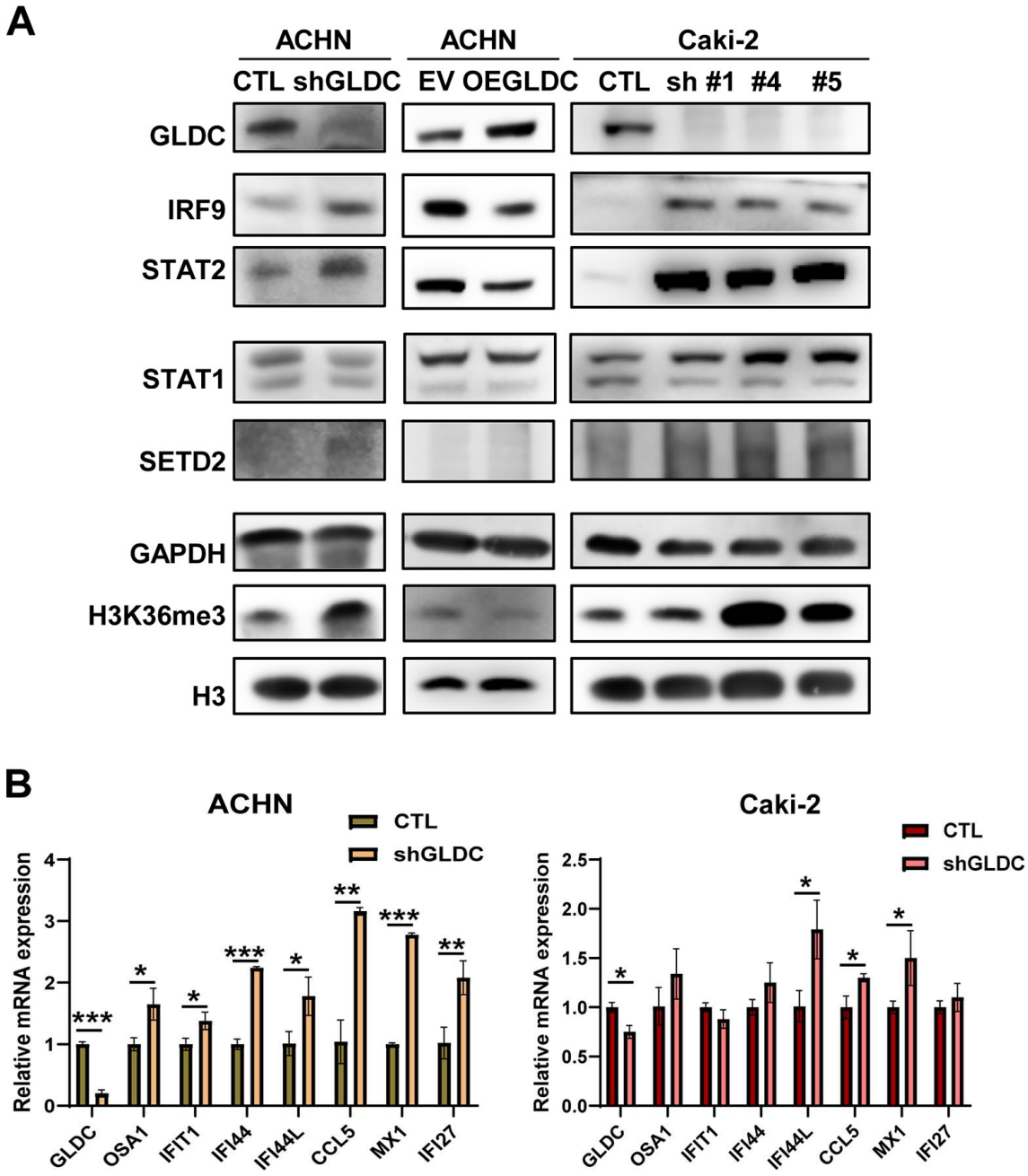

Figure 5. Knockdown of GLDC induces the activation of ISGF3 pathway. (A) Western blot analysis of indicated proteins in ACHN and Caki-2 cells. (B) mRNA levels of ISGs target genes: OSA1, IFIT1, IFI44, IFI44L, CCL5, MX1, IFI27 in indicated cells. Data are represented as the

mean ± SD (n = 3). Significant levels are indicated as follows: * $p < 0.05$, ** $p < 0.01$, and *** $p < 0.001$. CCL5: C-C motif chemokine ligand 5; IFI27: interferon alpha-inducible protein 27; IFI44: interferon induced protein 44; IFI44L: interferon-induced protein 44-like; IFIT1: interferon-induced protein with tetratricopeptide repeats 1; IRF9: interferon regulatory factor 9; ISFS3: interferon-stimulated gene factor 3; ISGs: interferon stimulated genes; MX1: MX dynamin like GTPase 1; OAS1: 2'-5'-oligoadenylate synthetase 1; OE: overexpression of GLDC; SETD2: SET domain containing 2; shGLDC: knockdown of GLDC; STAT1: signal transducer and activator of transcription 1; STAT2: signal transducer and activator of transcription 2; H3K36me3: histone 3 lysine 36 trimethylation; EV: corresponding control of OE GLDC.

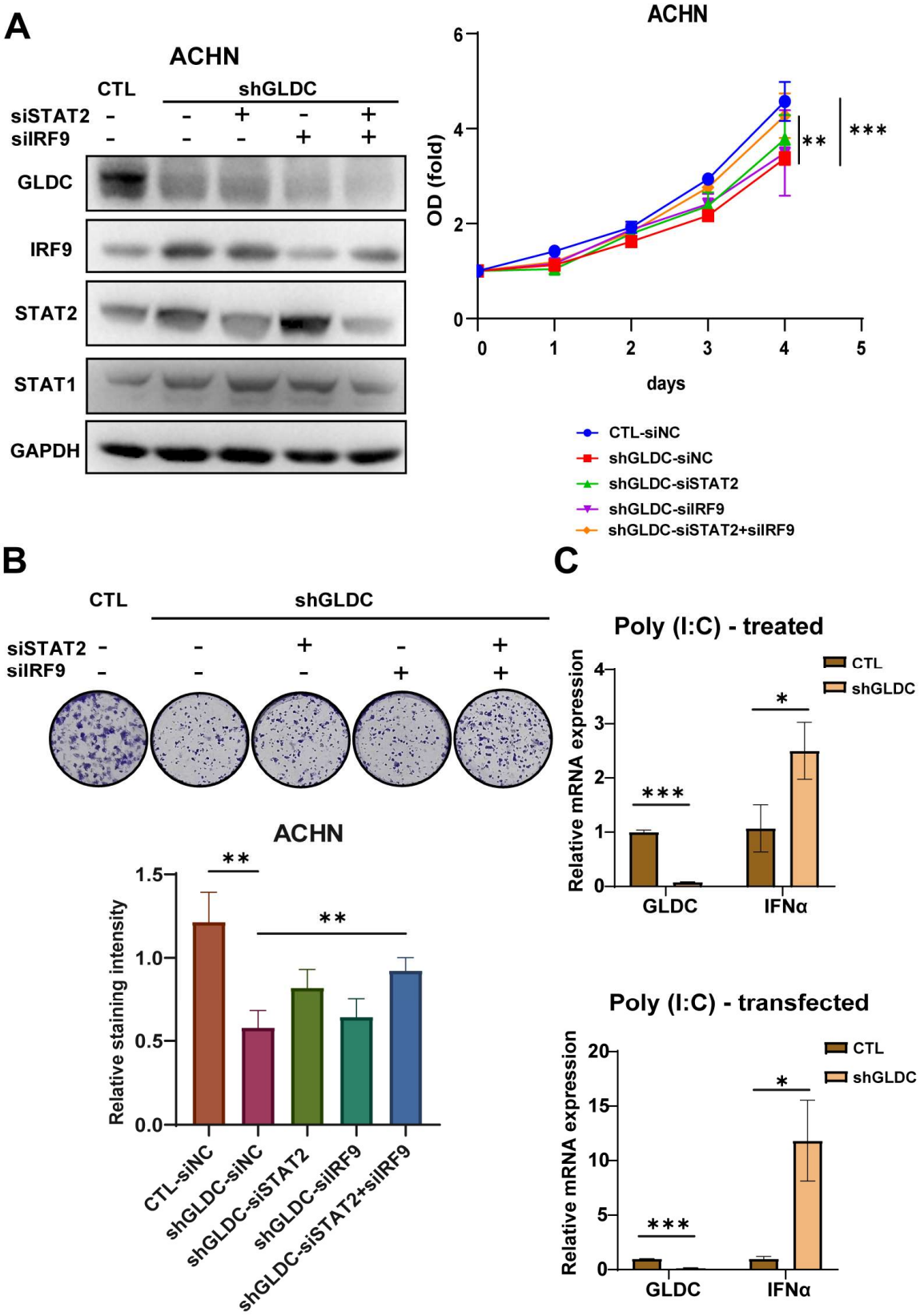

Figure 6. Downregulation of ISGF3 subunits reverses the decreased cell proliferation and colony formation induced by GLDC depletion. (A) Western blot analysis to confirm co-knockdown of STAT2 and/or IRF9 in ACHN shGLDC cells and cell proliferation assay in indicated cells (B) Colony assay of indicated cells. To quantify staining intensity, methanol was used to dissolve crystal violet-stained cells, and the absorbance was measured at a wavelength of 570 nm. (C) mRNA level of IFNα in ACHN CTL and shGLDC cells after treatment or transfection of Poly (I:C) for 24 h. Data are represented as the mean ± SD (n = 3). Significant levels are indicated as follows: * $p < 0.05$, ** $p < 0.01$, and *** $p < 0.001$. CTL: control; IFNα: interferon alpha; IRF9: interferon regulatory factor 9; ISGF3: interferon-stimulated gene factor 3; Poly (I:C): polyinosinic: polycytidylic acid; shGLDC: knockdown of GLDC; STAT1: signal transducer and activator of transcription 1; STAT2: signal transducer and activator of transcription 2.

A

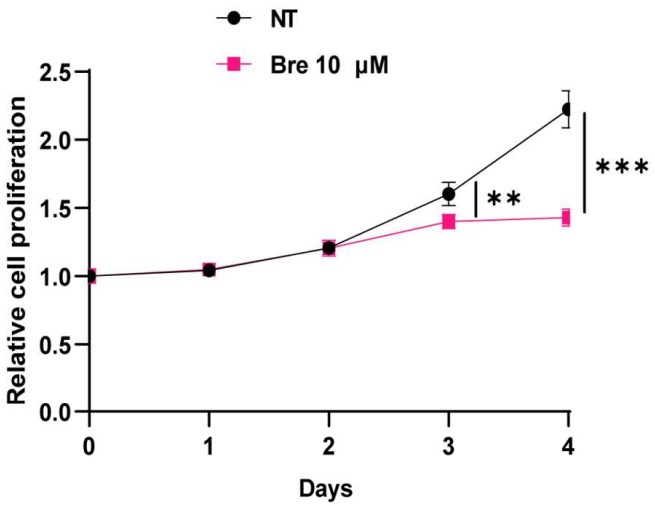

B

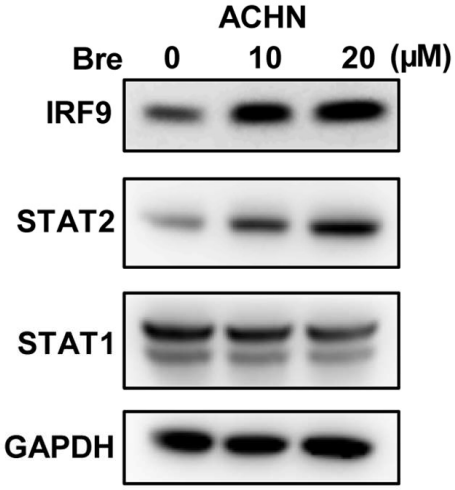

C

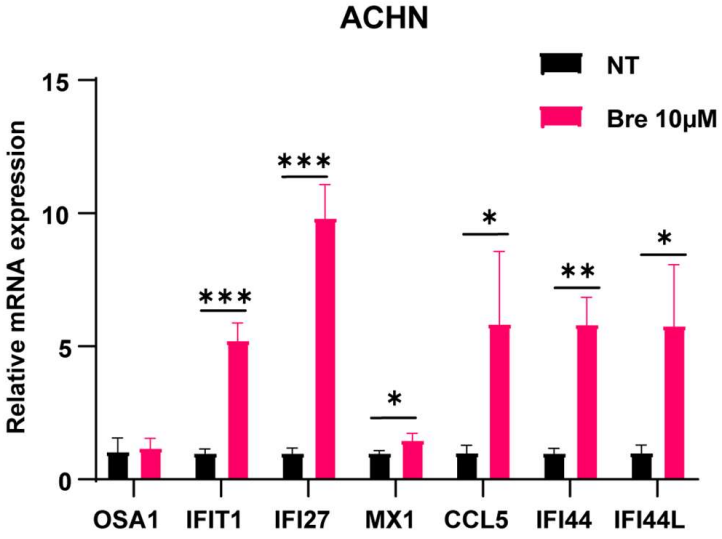

Figure 7. Inhibition of dNTPs synthesis induced by Bre suppresses cell proliferation and activates ISGF3 pathway. (A) ACHN cell proliferation with or without treatment of Bre 10 μM. (B) Protein expression of ISGF3 subunits in ACHN cell treated with Bre 10 μM or 20 μM. (C) mRNA of ISGs target genes in indicated cells. Data are represented as the mean ± SD (n = 3). Significant levels are indicated as follows: * $p < 0.05$, ** $p < 0.01$, and *** $p < 0.001$. Brequinar: Bre; CCL5: C-C motif chemokine ligand 5; IFI27: interferon alpha-inducible protein 27; IFI44: interferon induced protein 44; IFI44L: interferon-induced protein 44-like; IFIT1: interferon-induced protein with tetratricopeptide repeats 1; IRF9: interferon regulatory factor 9; ISFS3: interferon-stimulated gene factor 3; ISGs: interferon-stimulated genes; MX1: MX dynamin like GTPase 1; NT: non-treatment; OAS1: 2'-5'-oligoadenylate synthetase 1; STAT1: signal transducer and activator of transcription 1; STAT2: signal transducer and activator of transcription 2.

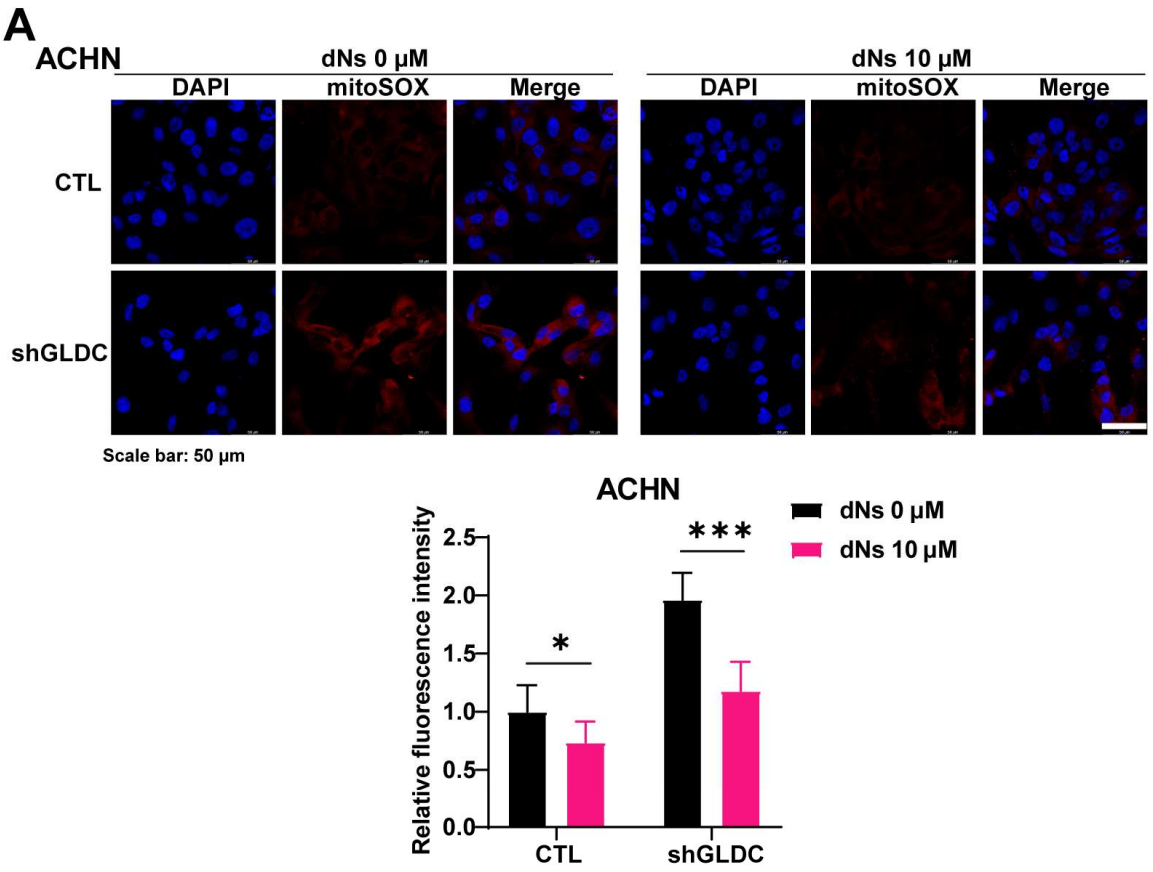

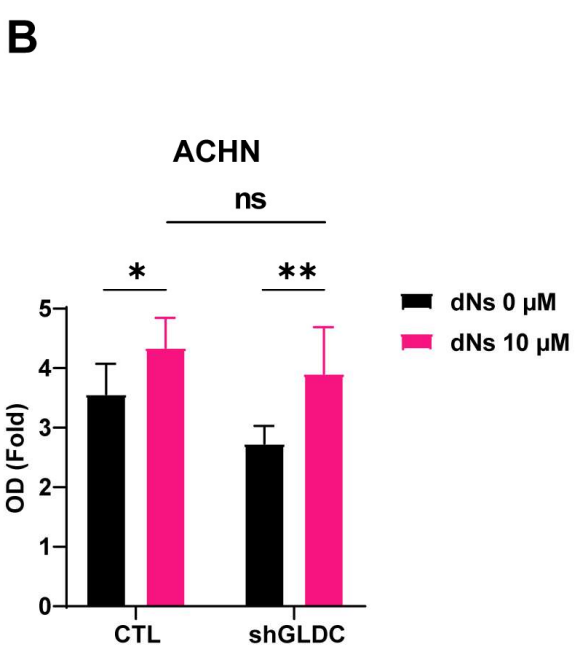

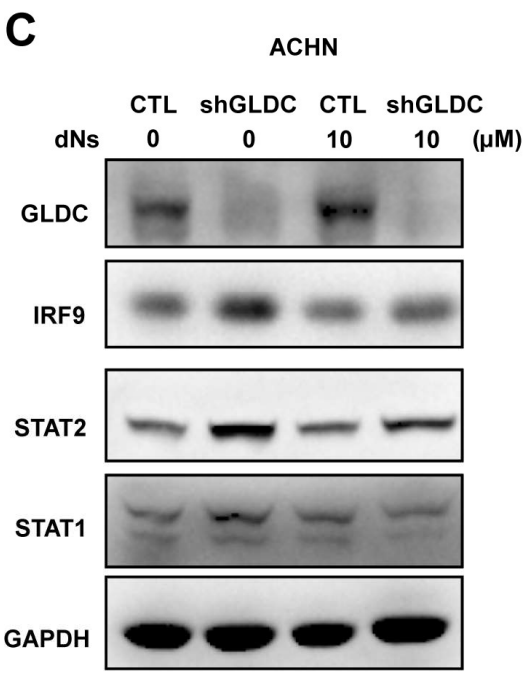

Figure 8. Addition of dNs restores the decreased cell proliferation and reduced expression of ISGF3 subunits in GLDC-depleted cells. (A) Representative fluorescence images of mitoSOX in ACHN CTL and shGLDC cells after 48 h of treatment with each dNs 10 μM and EHNA 5 μM. (B) Cellular growth of indicated cells after addition of each dNs 10 μM and EHNA 5 μM for 48 h. (C) Protein expression of ISGF3 subunits in indicated cells after 48 h of the treatment with each dNs 10 μM and EHNA 5 μM for 48 h. EHNA was added to prevent the degradation of deoxyadenosine. Data are represented as the mean ± SD (n = 3). Significant levels are indicated as follows: * $p < 0.05$, ** $p < 0.01$, *** $p < 0.001$, and ns: not significant. CTL: control; DAPI: 4',6-diamidino-2-phenylindole; dNs: deoxynucleosides; EHNA: erythro-9-(2-hydroxy-3-nonly) adenine; ISGF3: interferon-stimulated gene factor 3; IRF9: interferon regulatory factor 9; shGLDC: knockdown of GLDC; STAT1: signal transducer and activator of transcription 1; STAT2: signal transducer and activator of transcription 2.

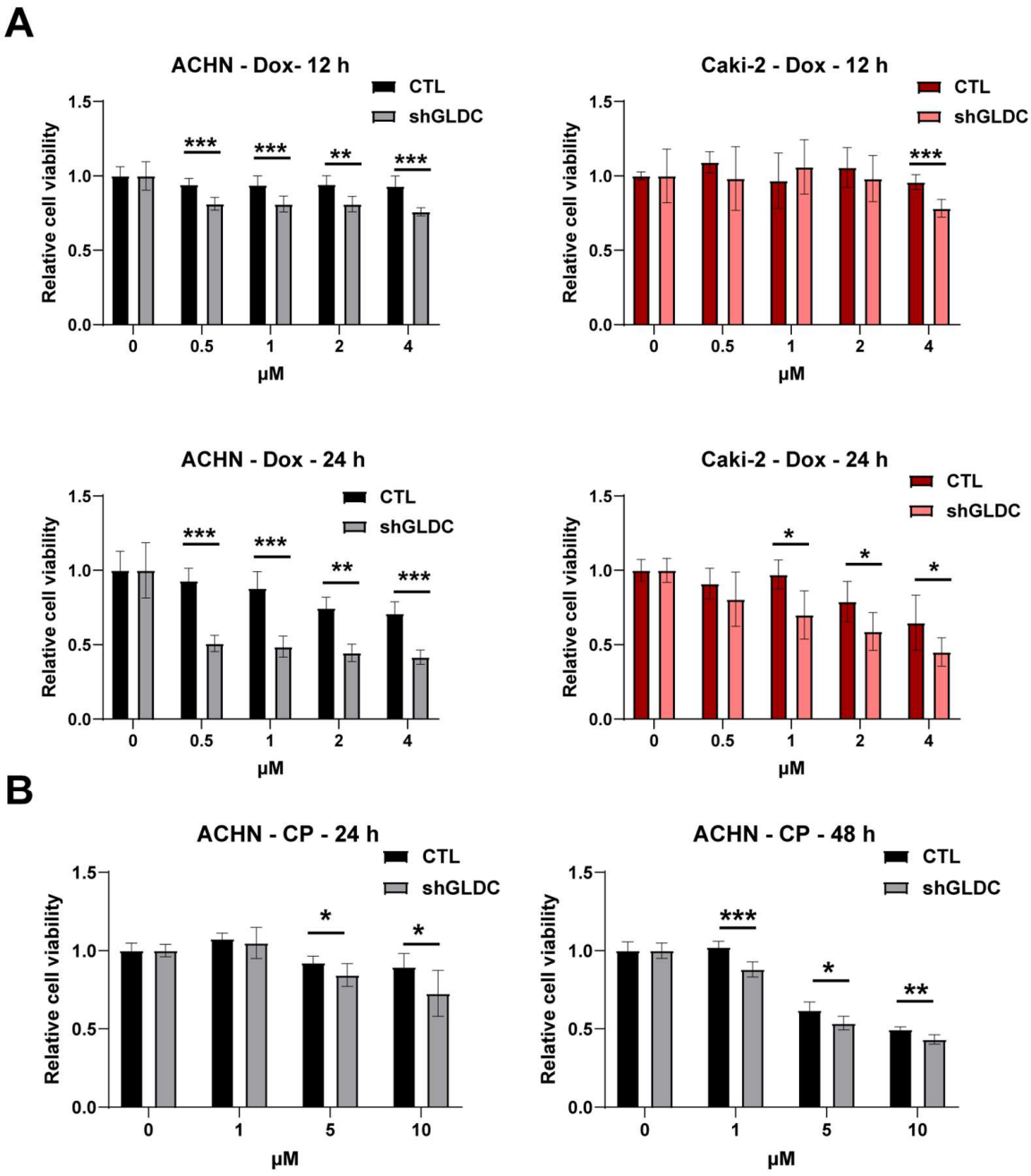

Figure 9. Depletion of GLDC decreases cell viability induced by Dox or CP in RCC cells. (A) Cell viability of indicated cells after treatment of Dox for 12 h or 24 h and (B) CP for

24 h or 48 h. Data are represented as the mean ± SD (n = 3). Significant levels are indicated as follows: * p < 0.05, ** p < 0.01, and *** p < 0.001. CTL: control; CP: cisplatin; Dox: doxorubicin; shGLDC: knockdown of GLDC.

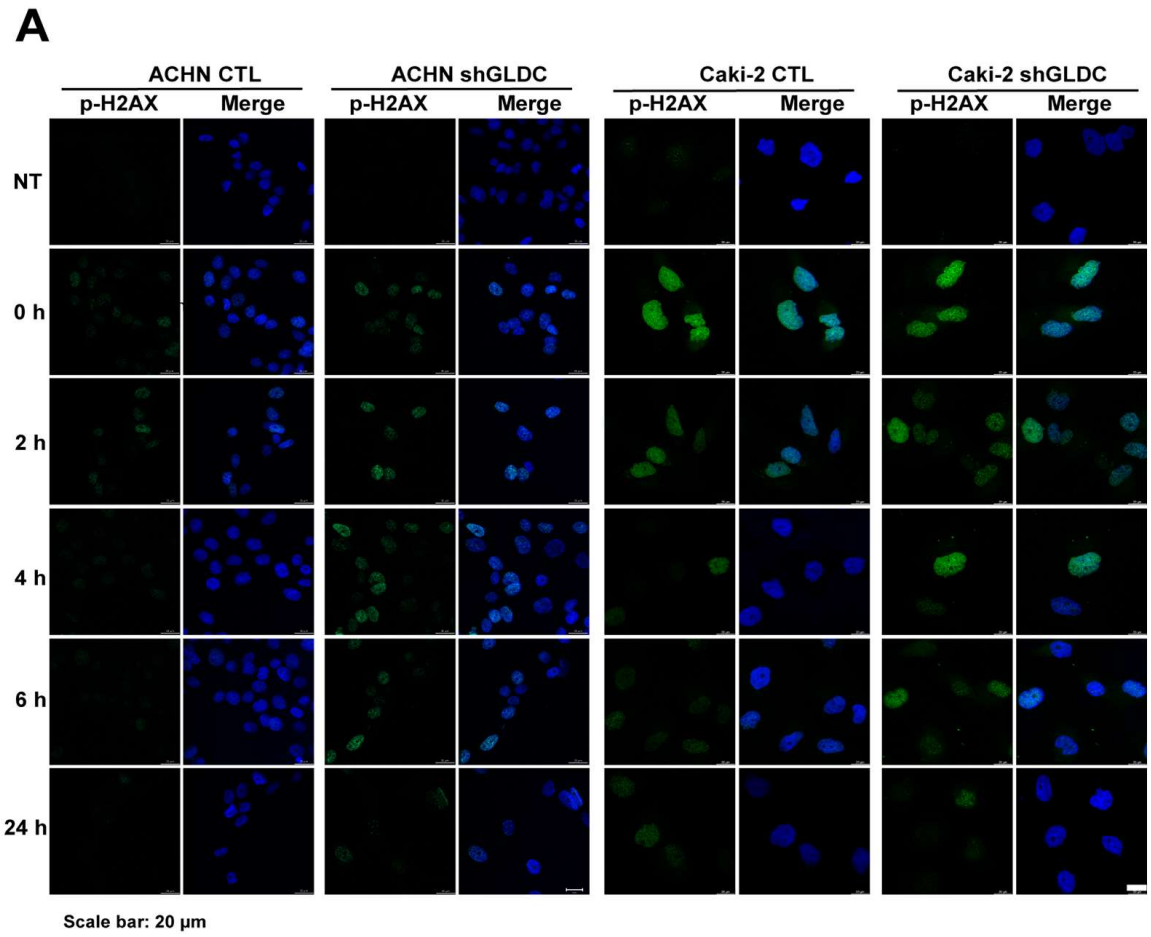

Figure 10. Depletion of GLDC augments DNA damage induced by Dox or CP in RCC cells. (A) Representative fluorescence images of indicated cells stained with anti-p-H2AX after 12 h of treatment of Dox 1 μM, followed by the release

into fresh media from 0 h to 24 h. (B) Protein expression of p-H2AX in indicated cells after 12 h of treatment of Dox 1 μM, followed by the release into fresh media from 0 h to 24 h. CTL: control; CP: cisplatin; Dox: doxorubicin; NT: non-treatment; p-H2AX: phospho-histone H2AX; shGLDC: knockdown of GLDC.

A

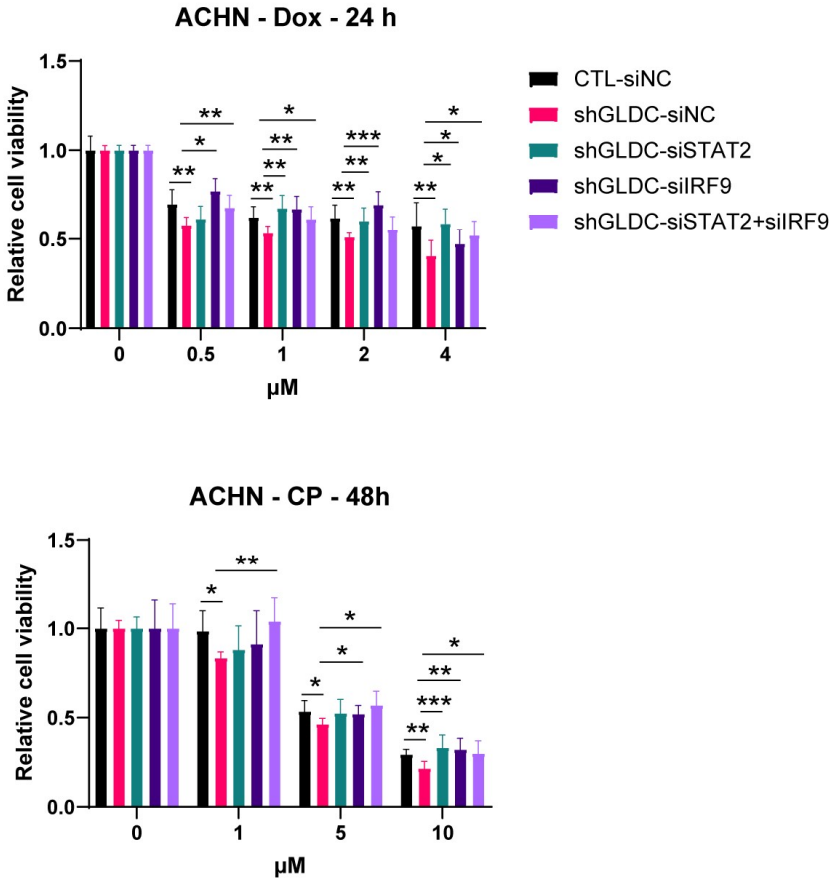

(continued)

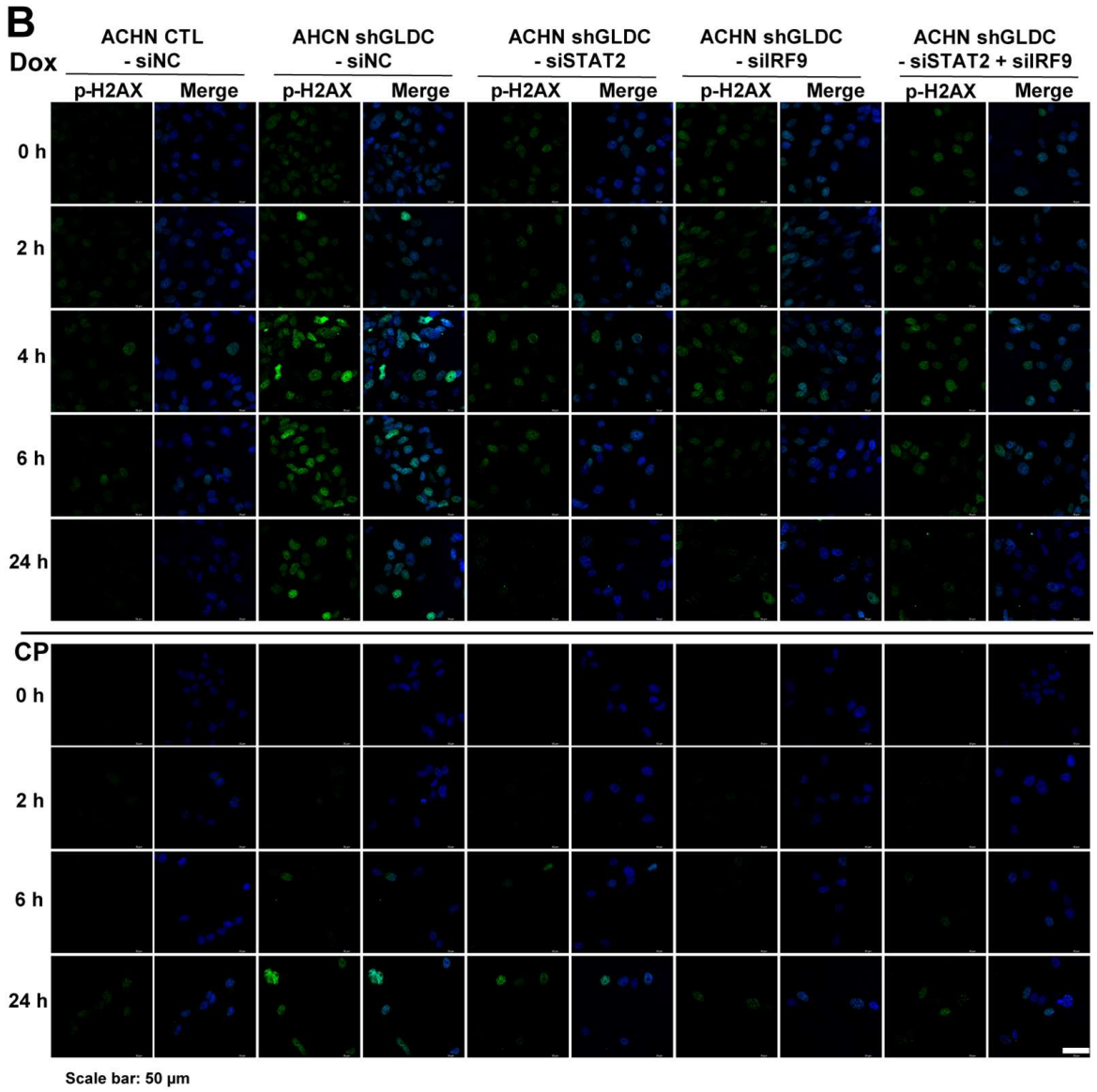

Figure 11. Knockdown of ISGF3 subunits reduces Dox or CP-induced DNA damage in GLDC-depleted cells. (A) Cell viability of indicated cells after 24 h and 48 h of treatment with Dox or CP, respectively. (B) Representative fluorescence images of indicated cells stained with anti-p-H2AX after 12 h of treatment with Dox 1 μM or 24 h of 10 μM CP, followed by the release into fresh media from 0 h to 24 h. Data are

represented as the mean ± SD (n = 3). Significant levels are indicated as follows: * $p < 0.05$, ** $p < 0.01$, and *** $p < 0.001$. CTL: control; CP: cisplatin; Dox: doxorubicin; p-H2AX: phospho-histone H2AX; shGLDC: knockdown of GLDC.

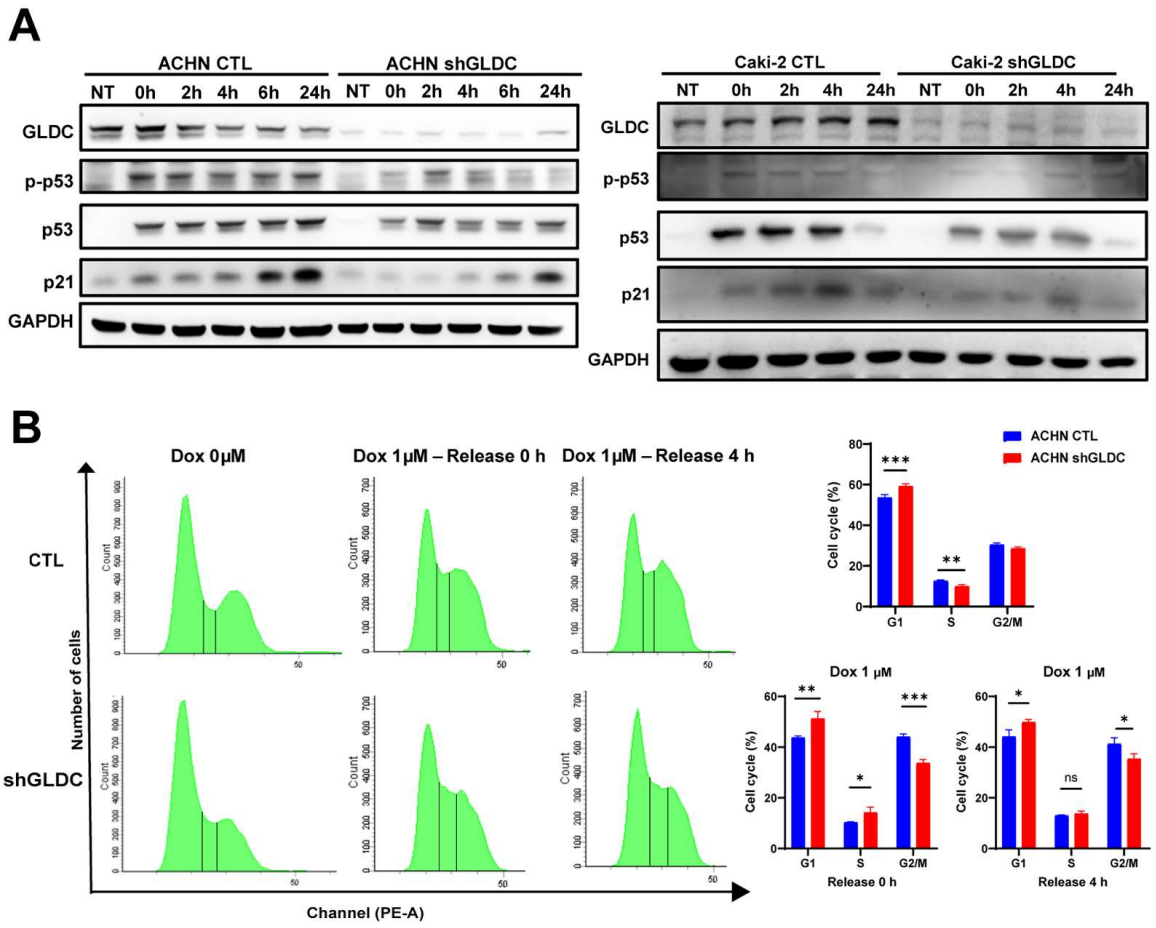

Figure 12. Knockdown of GLDC alleviates p53-dependent cell cycle checkpoint response to DNA damage. (A) Protein expression of p53, p-p53, p21 in indicated cells treated with Dox 1 μM for 12 h. (B) Cell cycle analysis of indicated cells treated with Dox 1 μM for 12 h followed by the release into fresh media for 4 h. Data are represented as the mean ± SD (n = 3). Significant levels are indicated as follows: * $p < 0.05$, ** $p < 0.01$, *** $p < 0.001$, and ns: not significant. CTL: control; Dox: doxorubicin; NT: non-treatment; p-H2AX: phospho-histone H2AX; p21: cyclin-dependent kinase inhibitor 1A; p-p53: phospho-tumor protein p53; p53:

tumor protein p53; shGLDC: knockdown of GLDC.

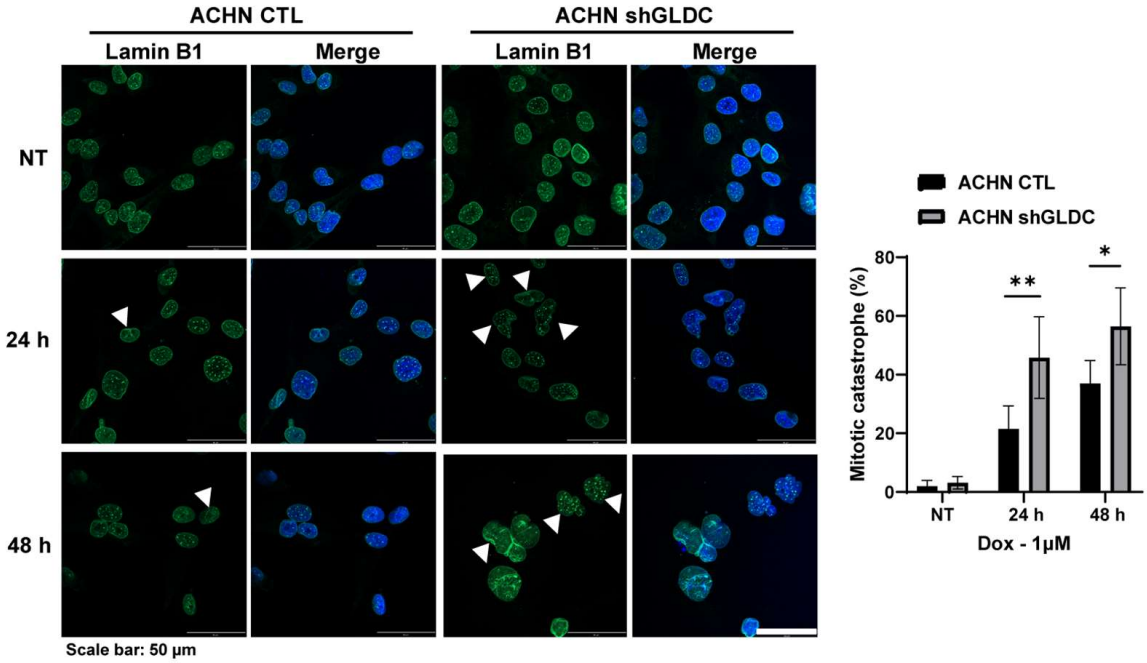

Figure 13. Knockdown of GLDC aggravates Dox-induced mitotic catastrophe in RCC cells. Representative fluorescence images of indicated cells treated with Dox for 24 h or 48 h. White triangles indicate cells undergoing mitotic catastrophe. Data are represented as the mean ± SD (n = 3). Significant levels are indicated as follows: * $p < 0.05$ and ** $p < 0.01$. CTL: control; Dox: doxorubicin; NT: non-treatment; shGLDC: knockdown of GLDC.

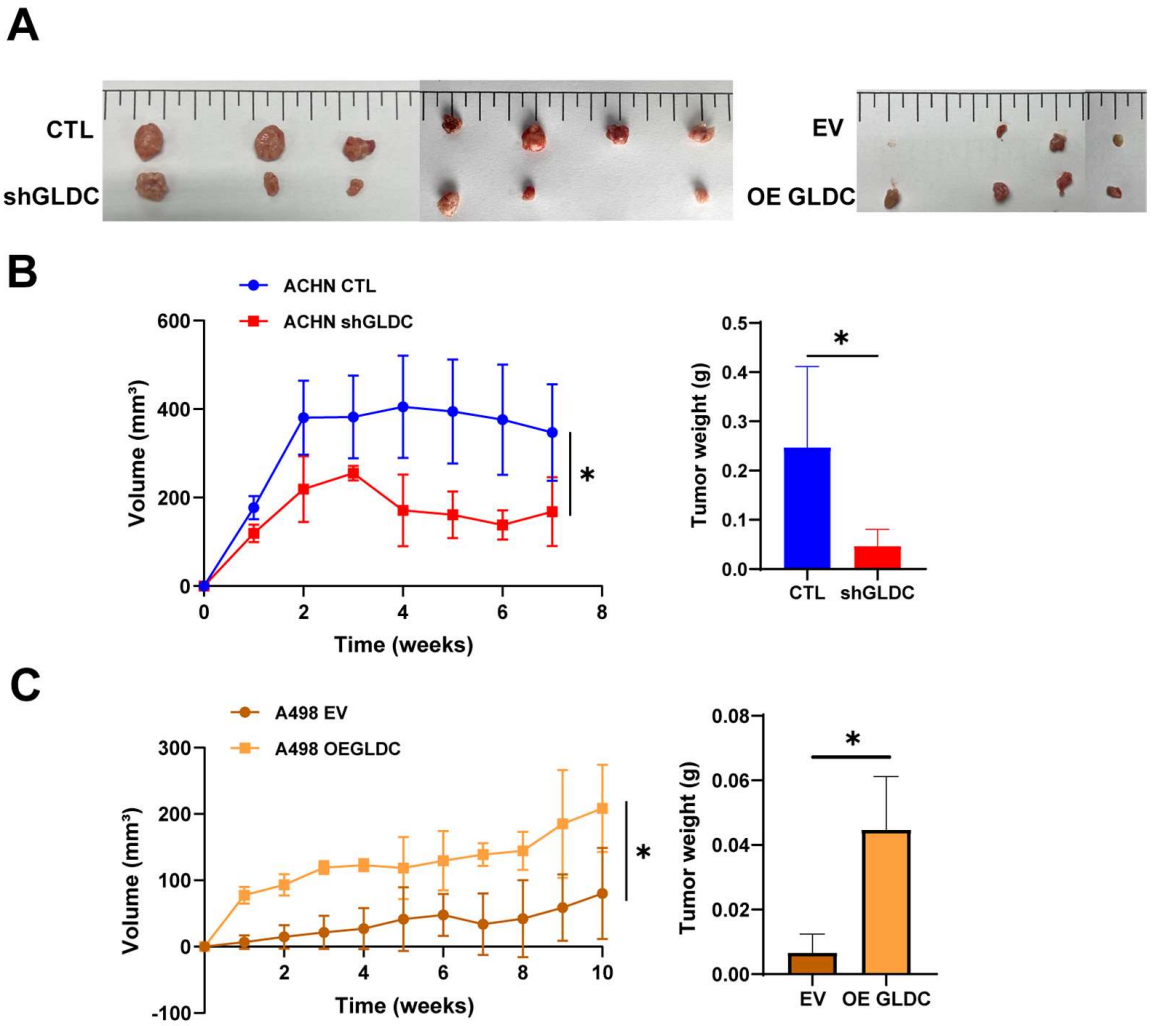

(continued)

D

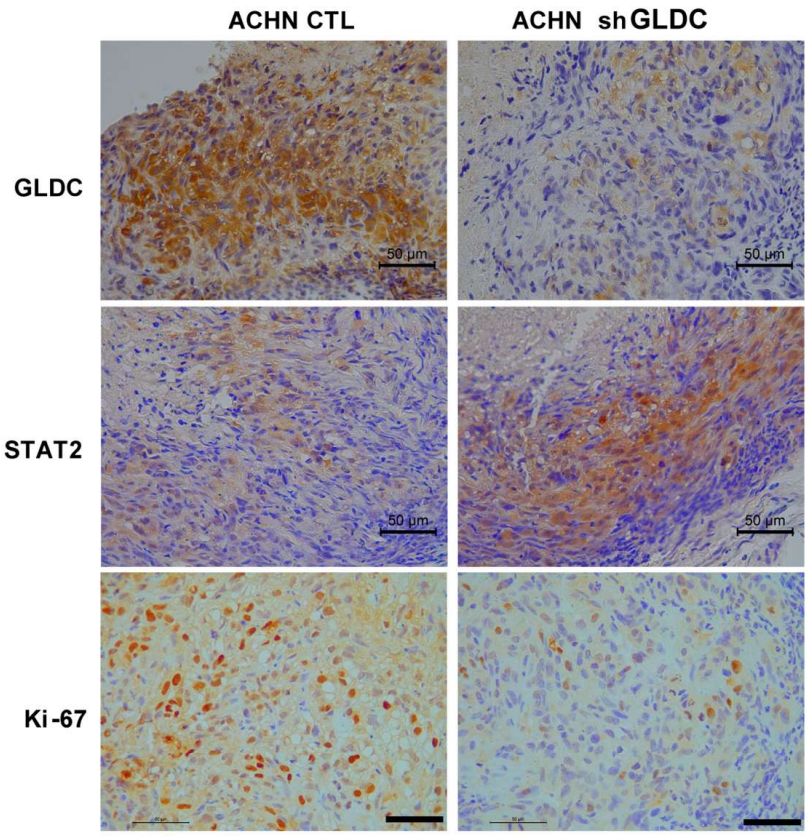

Scale bar: 50 μm

E

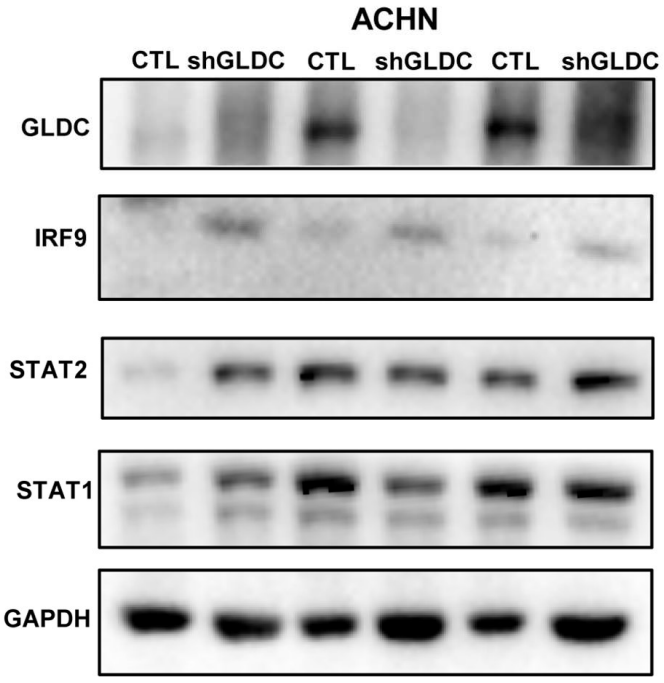

Figure 14. GLDC regulates RCC progression *in vivo*. (A) Images of xenograft tumors derived from ACHN CTL and shGLDC cells (n = 7) or from A498 EV and OE GLDC cells (n = 4). (B&C) Tumor volume and tumor weight of indicated cells. (D) Immunohistochemistry and (E) western blot analysis of indicated proteins of tumor tissues injected with ACHN CTL and shGLDC cells. Significant levels are indicated as follows: * $p < 0.05$. CTL: control; EV: corresponding control of OE GLDC; ISGF3: interferon-stimulated gene factor 3; IRF9: interferon regulatory factor 9; OE: overexpression of GLDC; shGLDC: knockdown of GLDC; STAT1: signal transducer and activator of transcription 1; STAT2: signal transducer and activator of transcription 2.

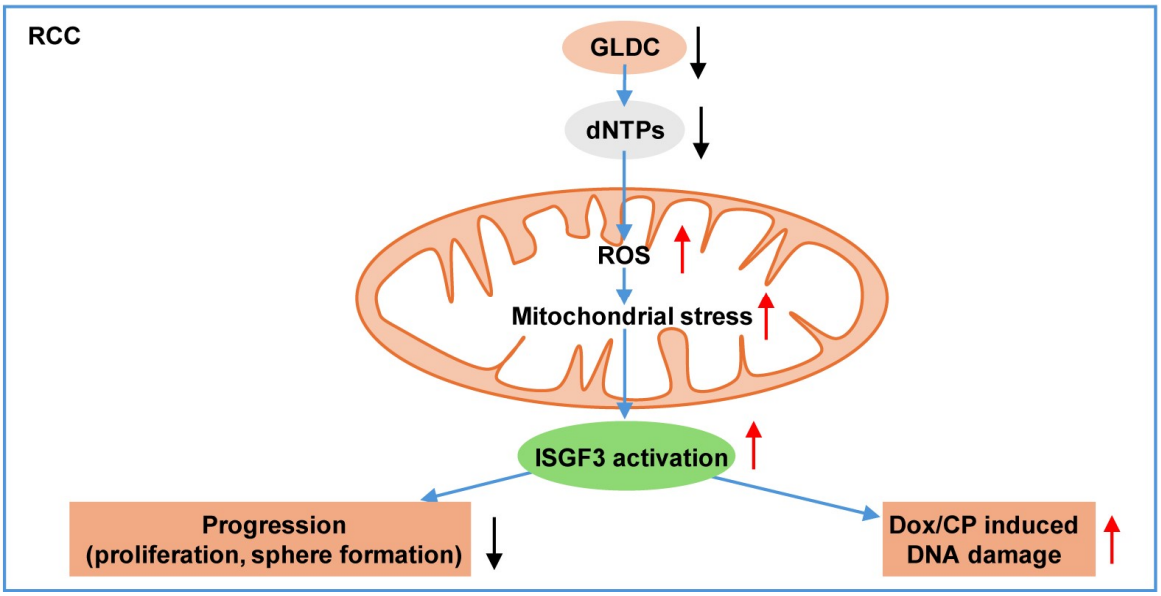

Figure 15. Schematic representation of mechanism by which GLDC regulates RCC progression. Knockdown of GLDC suppresses nucleotide synthesis, which increases ROS level and mitochondrial stress, activates ISGF3 complex, and ultimately regulates RCC progression and Dox or CP-induced DNA damage. CP: cisplatin; Dox: doxorubicin; dNTPs: deoxynucleotide triphosphates; ISGF3: interferon-stimulated gene factor 3; RCC: renal cell carcinoma; ROS: reactive oxygen species.

4. Discussion

This study identifies that GLDC might be a promising target for RCC therapy. I demonstrated that knockdown of GLDC depletes nucleotide synthesis, inducing ROS accumulation. This accumulation of ROS subsequently triggers mitochondrial stress, leading to decreased RCC cell proliferation and suppressed tumor growth. Conversely, overexpression of GLDC increases cell proliferation and promotes tumor growth. Restoration of dNs in GLDC-deficient cells dampens ROS production and reverses decreased cell proliferation in this cell line. Mechanically, suppression of GLDC increased protein expression of STAT2 and IRF9, two subunits of ISGF3 complex, subsequently augmenting mRNA expression of ISGs target genes. Co-knockdown of STAT2 and IRF9 restores the suppressed cellular proliferation induced by GLDC depletion. Additionally, knockdown of GLDC exacerbates Dox or CP-induced DNA damage via ISGF3 complex. Overall, these results demonstrate that GLDC acts as an oncogene in RCC progression, and it could be a promising therapeutic candidate for RCC treatment.

The understanding of the function of GLDC regarding tumorigenesis has been limited. While GLDC has been shown to make a clear contribution to the initiation of NSCLC (12,28), its role in HCC remains contradictory. Previous studies reveal that GLDC-deficient Huh7 cells promote metastasis *in vitro* and orthotopic mice model and GLDC-overexpressing HCCLM3 cells reverse these effects (11,29), suggesting a tumor-suppressive role for GLDC in HCC. However, a recent study suggests that GLDC could be an oncogene in HCC as GLDC depletion suppresses HCC

cell proliferation and tumor growth (30). These findings indicate that the function of GLDC in tumorigenesis can differ even within the same cancer type. In this paper, I demonstrated that GLDC acts as an oncogene in ACHN and Caki-2 RCC cells.

Previous studies reveal that cancer cells exhibit enhanced generation and utilization of nucleotides, which are essential for cell proliferation and replication (9). Nucleotide synthesis pathway has been shown to involve various oncogenes, such as MYC, phosphatidylinositol 3-kinase (PI3K), and mutant KRAS proto-oncogene, GTPase (KRAS) (31-33). Therefore, numerous studies have focused on identifying potential targets related to this pathway for cancer therapy. Aside from 5-fluorouracil, therapeutic agents aimed at nucleotide synthesis have had limited success. GLDC is a mitochondrial enzyme that is a part of GCS. Its activity contributes to the production of 5,10-meTHF, a molecule that plays a crucial role in nucleotide biosynthesis. Based on this, I proposed that GLDC might impact nucleotide synthesis, thereby regulating RCC progression and providing a potential strategy for RCC treatment. The results from this study reveal that GLDC depletion reduces dNTP levels and cellular proliferation in RCC cells, which aligns with the effects observed with Bre treatment. Moreover, addition of dNs into GLDC-depleted cells mitigates the decreased cell proliferation induced by GLDC knockdown. These results suggest that GLDC regulates RCC cell proliferation by adjusting nucleotide synthesis.

Apart from its catalytic function in glycine metabolism, GLDC is involved in the regulation of ROS generation (11,29). Thus, ROS production was evaluated following the depletion of GLDC in RCC cells and the results show that knockdown of GLDC and suppression of nucleotide synthesis with Bre treatment lead to increased ROS

production. On the other hand, addition of dNs in GLDC-depleted cells not only decreases ROS level but also increases cell proliferation. These results indicate that reduced nucleotide synthesis induced by GLDC knockdown results in elevated ROS generation and diminished cell proliferation.

5. Summary

This study aims to determine whether GLDC could have a crucial role in RCC progression. Knockdown of GLDC decreases intracellular dNTP pools, which induces increased ROS production. This elevated ROS level triggers mitochondrial stress, resulting in the activation of ISGF3 pathway, which ultimately inhibits RCC cell progression and mitigates tumor growth in mice injected with RCC cells. Moreover, addition of dNs dampens the increased ROS production, decreased cellular proliferation, and increased ISGF3 subunits expression in GLDC-depleted cells. Based on these results, this study indicates that GLDC might be a promising target for RCC therapy.

References

1. Barata PC, Rini BI: Treatment of renal cell carcinoma: Current status and future directions. CA Cancer J Clin 2017; 67(6): 507-24.

2. Motzer RJ, Hutson TE, Cella D, Reeves J, Hawkins R, Guo J, et al.: Pazopanib versus sunitinib in metastatic renal cell carcinoma. N Engl J Med 2013; 369(8): 722-31.

3. Huang CY, Yagüe-Capilla M, González-Pacanowska D, Chang ZF: Quantitation of deoxynucleoside triphosphates by click reactions. Sci Rep 2020; 10(1): 611-21.

4. Traut TW: Physiological concentrations of purines and pyrimidines. Mol Cell Biochem 1994; 140(1): 1-22.

5. Dong Y, Tu R, Liu H, Qing G: Regulation of cancer cell metabolism: oncogenic MYC in the driver's seat. Signal Transduct Target Ther 2020; 5(1): 124-35.

6. Berlin J, Benson AB 3rd: Chemotherapy: Gemcitabine remains the standard of care for pancreatic cancer. Nat Rev Clin Oncol 2010; 7(3): 135-7.

7. Longley DB, Harkin DP, Johnston PG: 5-fluorouracil: mechanisms of action and clinical strategies. Nat Rev Cancer 2003; 3(5): 330-8.

8. Foekens JA, Romain S, Look MP, Martin PM, Klijn JG: Thymidine kinase and thymidylate synthase in advanced breast cancer: response to tamoxifen and chemotherapy. Cancer Res 2001; 61(4): 1421-5.

9. Mullen NJ, Singh PK: Nucleotide metabolism: a pan-cancer metabolic dependency. Nat Rev Cancer 2023; 23(5): 275-94.

10. Tibbetts AS, Appling DR: Compartmentalization of mammalian folate-mediated one-carbon metabolism. Annu Rev Nutr 2010; 30: 57-81.

11. Zhuang H, Wu F, Wei W, Dang Y, Yang B, Ma X, et al.: Glycine decarboxylase induces autophagy and is downregulated by miRNA-30d-5p in hepatocellular carcinoma. Cell Death Dis 2019; 10(3): 192-206.

12. Zhang WC, Shyh-Chang N, Yang H, Rai A, Umashankar S, Ma S, et al.: Glycine decarboxylase activity drives non-small cell lung cancer tumor-initiating cells and tumorigenesis. Cell 2012; 148(1-2): 259-72.

13. Chen MK, Xiao ZY, Huang ZP, Xue KY, Xia H, Zhou JW, et al.: Glycine Decarboxylase (GLDC) plays a crucial role in regulating energy metabolism, invasion, metastasis and immune escape for prostate cancer. Int J Biol Sci 2023; 19(15): 4726-43.

14. Vella V, De Francesco EM, Bonavita E, Lappano R, Belfiore A: IFN-I signaling in cancer: the connection with dysregulated

Insulin/IGF axis. Trends Endocrinol Metab 2022; 33(8): 569-86.

15. Cheon H, Wang Y, Wightman SM, Jackson MW, Stark GR: How cancer cells make and respond to interferon-I. Trends Cancer 2023; 9(1): 83-92.

16. Liao L, Liu ZZ, Langbein L, Cai W, Cho EA, Na J, et al.: Multiple tumor suppressors regulate a HIF-dependent negative feedback loop via ISGF3 in human clear cell renal cancer. Elife 2018; 7: 7925-51.

17. Wu Z, Oeck S, West AP, Mangalhara KC, Sainz AG, Newman LE, et al.: Mitochondrial DNA stress signalling protects the nuclear genome. Nature Metabolism 2019; 1(12): 1209-18.

18. Zhou J, Wang D, Wong BH, Li C, Poon VK, Wen L, et al.: Identification and characterization of GLDC as host susceptibility gene to severe influenza. EMBO Mol Med 2019; 11(1): 9528-42.

19. Purhonen J, Banerjee R, McDonald AE, Fellman V, Kallijärvi J: A sensitive assay for dNTPs based on long synthetic oligonucleotides, EvaGreen dye and inhibitor-resistant high-fidelity DNA polymerase. Nucleic Acids Res 2020; 48(15): 87-104.

20. Hiraga K, Kikuchi G: The mitochondrial glycine cleavage system. Functional association of glycine decarboxylase and aminomethyl carrier protein. J Biol Chem 1980; 255(24): 11671-6.

21. Jain M, Nilsson R, Sharma S, Madhusudhan N, Kitami T, Souza AL, et al.: Metabolite profiling identifies a key role for glycine in rapid cancer cell proliferation. Science 2012; 336(6084): 1040-4.

22. Fang J, Uchiumi T, Yagi M, Matsumoto S, Amamoto R, Takazaki S, et al.: Dihydro-orotate dehydrogenase is physically associated with the respiratory complex and its loss leads to mitochondrial dysfunction. Biosci Rep 2013; 33(2): 217-28.

23. Winberg F, Hamanaka R, Wheaton WW, Winberg S, Joseph J, Lopez M, et al.: Mitochondrial metabolism and ROS generation are essential for Kras-mediated tumorigenicity. Proc Natl Acad Sci USA 2010; 107(19): 8788-93.

24. West AP, Khoury-Hanold W, Staron M, Tal MC, Pineda CM, Lang SM, et al.: Mitochondrial DNA stress primes the antiviral innate immune response. Nature 2015; 520(7548): 553-7.

25. Cheon H, Holvey-Bates EG, Schoggins JW, Forster S, Hertzog P, Imanaka N, et al.: IFNβ-dependent increases in STAT1, STAT2, and IRF9 mediate resistance to viruses and DNA damage. Embo J 2013; 32(20): 2751-63.

26. Carvalho S, Vítor AC, Sridhara SC, Martins FB, Raposo AC, Desterro JM, et al.: SETD2 is required for DNA double-strand break repair and activation of the p53-mediated checkpoint. Elife 2014; 3: 2482-501.

27. Lavin MF, Gueven N: The complexity of p53 stabilization and

activation. Cell Death & Differ 2006; 13(6): 941-50.

28. Yuan Y, Sun L, Wang X, Chen J, Jia M, Zou Y, et al.: Identification of a new GLDC gene alternative splicing variant and its protumorigenic roles in lung cancer. Future Oncol 2019; 15(36): 4127-39.

29. Zhuang H, Li Q, Zhang X, Ma X, Wang Z, Liu Y, et al.: Downregulation of glycine decarboxylase enhanced cofilin-mediated migration in hepatocellular carcinoma cells. Free Radic Biol Med 2018; 120: 1-12.

30. Mukha D, Fokra M, Feldman A, Sarvin B, Sarvin N, Nevo-Dinur K, et al.: Glycine decarboxylase maintains mitochondrial protein lipoylation to support tumor growth. Cell Metab 2022; 34(5): 775-82.

31. Santana-Codina N, Roeth AA, Zhang Y, Yang A, Mashadova O, Asara JM, et al.: Oncogenic KRAS supports pancreatic cancer through regulation of nucleotide synthesis. Nat Commun 2018; 9(1): 4945-58.

32. Hoxhaj G, Manning BD: The PI3K-AKT network at the interface of oncogenic signalling and cancer metabolism. Nat Rev Cancer 2020; 20(2): 74-88.

33. Liu YC, Li F, Handler J, Huang CR, Xiang Y, Neretti N, et al.: Global regulation of nucleotide biosynthetic genes by c-Myc. PLoS One 2008; 3(7): 2722-35.

Glycine Decarboxylase Regulates Renal Carcinoma Progression via Interferon-Stimulated Gene Factor 3-Mediated Pathway

Pham, Thi Tuyet Mai

Department of Biochemistry
Graduate School

Keimyung University

(Suppervised by Professor Ha, Eun Young)

(Abstract)

Renal cell carcinoma (RCC) has recently been classified as a metabolic disease due to the reprogramming of various metabolic pathways that drive cancer development. Glycine decarboxylase (GLDC) is one of the enzymes in glycine cleavage system, which transfers one-carbon units for nucleotide synthesis. This study aims to elucidate the function of GLDC in RCC progression. Knockdown of GLDC depleted nucleotide synthesis and led to reactive oxygen species (ROS) generation, triggering mitochondrial stress and then activating interferon-stimulated gene factor 3 (ISGF3) pathway. Hence, GLDC depletion suppressed cellular proliferation and tumor growth, while overexpression of GLDC reversed these effects in

RCC cells. Particularly, GLDC depletion increased expression of ISGF3 subunits, whereas GLDC overexpression decreased expression of this complex. Moreover, addition of deoxynucleoside (dNs) dampened the elevated ROS levels, mitigated expression of ISGF3 subunits, and ultimately enhanced cell proliferation, which aligns with the effect of knockdown ISGF3 subunits in GLDC-deficient cells. Further findings identify that knockdown of GLDC increased doxorubicin or cisplatin-induced damage through ISGF3 pathway activation. Overall, this study suggests that GLDC has an important function in RCC progression and offers a potential approach for RCC treatment.

Glycine Decarboxylase Regulates Renal Carcinoma Progression via Interferon-Stimulated Gene Factor 3-Mediated Pathway

Pham, Thi Tuyet Mai
계명대학교 대학원
의학과 생화학 전공
(지도교수 하 은 영)

(초록)

다양한 대사 경로의 reprogramming이 암발생에 기여한다는 연구 결과들의 발표로 인해 신장암(renal cell carcinoma, RCC)은 대사 질환으로 분류되기도 한다. 이러한 대사 경로의 reprogramming 변화는 암세포의 증식, 전이 및 화학요법 내성에 기여한다고 알려져 있다. Glycine decarboxylase (GLDC)는 글리신 분해 시스템에서 뉴클레오타이드 합성을 위한 일탄소 단위를 전달하는 핵심 효소 중 하나이다. 본 연구는 RCC 진행 과정에서 GLDC의 역할을 규명하는 것을 목표로 한다. 연구 결과, GLDC 발현 억제가 뉴클레오타이드 합성을 감소시키며, 활성 산소종(reactive oxygen species, ROS) 생성을 통해 미토콘드리아 스트레스를 유발하고 interferon-stimulated gene factor 3 (ISGF3) 경로를 활성화한다는 사실이 밝혀졌다. GLDC의 발현 억제는 RCC 세포에서 세포 증식과 종양 성장을 억제했으며, GLDC 과발현은 RCC 세포에서 세포 증식과 종양

성장을 증가시킨 것을 관찰하였다. 특히, GLDC 발현 억제 세포에서는 ISGF3의 구성요소 발현이 증가했지만, GLDC 과발현 세포에서는 감소하였다. 또한, deoxynucleosides (dNs) 추가 시 ROS 증가가 완화되고 ISGF3 구성요소 발현이 감소하며 세포 증식이 촉진되었다. 이는 GLDC 억제 세포에서의 ISGF3 억제 효과와 일치한다. 마지막으로, GLDC 억제는 ISGF3 경로 활성화를 통해 독소루비신 및 시스플라틴에 의한 세포 손상을 증가시켰다. 결론적으로, 본 연구는 GLDC가 RCC 진행을 조절하는 데 중요한 역할을 하며, RCC 치료를 위한 치료제 개발 가능성을 제시한다.

□ Biography

1996년 베트남 출생
계명대학교 대학원 의학 석사
계명대학교 의과대학 생화학교실 박사학위 대학원생(현)

□ Papers and books

「Antiviral Activities of High Energy E-Beam Induced Copper Nanoparticles against H1N1 Influenza Virus」 Nanomaterials (Basel) 2022. 01.